A Novel Balanced Arithmetic Optimization Algorithm Optimized Controller for Enhanced Voltage Regulation

Serdar Ekinci , Haluk Çetin , Davut Izci , Ercan Köse *

Posted Date: 7 November 2023

doi: 10.20944/preprints202311.0390.v1

Keywords: arithmetic optimization algorithm; elite opposition-based learning; pattern search; PIDND2N2 controller

Article

A Novel Balanced Arithmetic Optimization Algorithm Optimized Controller for Enhanced Voltage Regulation

Serdar Ekinci [1], Haluk Çetin [2], Davut Izci [3] and Ercan Köse [4,*]

[1] Department of Computer Engineering, Batman University; ekinciser@yahoo.com
[2] Institute of postgraduate Studies, Batman University; halukcetinbt@gmail.com
[3] Department of Computer Engineering, Batman University; davutizci@gmail.com
[4] Electrical-Electronics Engineering Department, Tarsus University; ekose@tarsus.edu.tr
* Correspondence: ekose@tarsus.edu.tr

Abstract: This work introduces an innovative approach that unites a PIDND²N² controller and the balanced arithmetic optimization algorithm (b-AOA) to enhance the stability of an automatic voltage regulator (AVR) system. The PIDND²N² controller, tailored for precision, stability, and responsiveness, mitigates the limitations of conventional methods. The b-AOA optimizer is obtained through integration of pattern search and elite opposition-based learning strategies into the arithmetic optimization algorithm. This integration optimizes the controller parameters and the AVR system's response, harmonizing exploration and exploitation. Extensive assessments, including evaluations on 23 classical benchmark functions, demonstrate the efficacy of the b-AOA. It consistently achieves accurate solutions, exhibits robustness in addressing a wide range of optimization problems, and stands out as a promising choice for various applications. In terms of AVR system, comparative analyses highlight the superiority of the proposed approach in transient response characteristics, with the shortest rise and settling times and zero overshoot. Additionally, the b-AOA approach excels in frequency response, ensuring robust stability and a broader bandwidth. Furthermore, the proposed approach is compared with various state-of-the-art control methods for the AVR system, showcasing impressive performance. These important results underscore the significance of this work, setting a new benchmark for AVR control by advancing stability, responsiveness, and reliability in power systems.

Keywords: arithmetic optimization algorithm; elite opposition-based learning; pattern search; PIDND²N² controller

1. Introduction

In the realm of power systems, the automatic voltage regulator (AVR) stands as a linchpin, ensuring that connected electrical equipment functions within prescribed voltage bounds. The consequences of inadequate voltage regulation can be profound, from equipment damage and operational failures to costly downtime and extensive repairs [1–3]. Consequently, the AVR plays a pivotal role in power systems reliant on generators or alternators for electricity generation. While existing control methodologies have achieved some success, they remain encumbered by limitations [4], including challenges related to robustness, overshoots, rise times, settling times, and persistent steady-state errors.

It is against this backdrop that our study emerges, driven by a shared motivation to push the boundaries of AVR control and contribute to the development of more robust and efficient power systems. Our primary motivation is to propose an advanced control scheme capable of effectively addressing these limitations. To realize this goal, we have developed a novel optimizer, rooted in the arithmetic optimization algorithm (AOA) [5], meticulously fine-tuned to enhance the parameters of our proposed control scheme and, by extension, its overall performance and adaptability.

In the existing landscape of AVR control, controllers have emerged as indispensable assets for vigilant monitoring and regulation of the AVR itself. These controllers serve as hubs, facilitating real-

 doi:10.20944/preprints202311.0390.v1

time adjustments to maintain voltage stability, enabling remote monitoring, fault detection, and automatic shutdown during emergencies, and enhancing the overall system dependability. A range of controllers, from the standard proportional-integral-derivative (PID) to more advanced variants like the PID Acceleration (PIDA), fractional-order PID (FOPID), and PID with a second-order derivative ($PIDD^2$), offer diverse attributes to meet the specific requirements of AVR control [6–13].

However, the choice of controller alone is insufficient to address the complex challenges faced by AVR systems. The choice of a cost function is equally crucial, as it significantly impacts performance. Researchers employ various cost functions, such as the integral of time-weighted squared error, integral of squared error, integral of absolute error, and the dynamic response performance criteria-based Zwe-Lee Gaing (ZLG) cost function [14–16].

In this context, our work introduces a novel approach that unites both the controller and the optimizer to form a comprehensive solution for enhancing AVR stability. The core innovation is the balanced arithmetic optimization algorithm (b-AOA). It marries the powerful pattern search (PS) strategy [17], renowned for its exploitation capabilities, with the elite opposition-based learning (EOBL) strategy [18], elevating exploration. This marriage optimizes the controller parameters and the AVR system's response, harmonizing exploration and exploitation to attain a level of stability previously out of reach.

The efficacy of the b-AOA is first verified through comprehensive assessments against 23 classical unimodal, multimodal, and fixed-dimensional multimodal benchmark functions. These evaluations compare the effectiveness of the proposed b-AOA algorithm to other optimization algorithms, including the original AOA [5], sine-cosine algorithm [19], weighted mean of vectors algorithm [20] and marine predators algorithm [21]. The results from the benchmark functions underscore the remarkable performance of the b-AOA algorithm. It consistently achieves mean errors close to zero, demonstrating its capability to find accurate solutions. Furthermore, its robustness and consistency make it a strong candidate for addressing a wide range of optimization problems.

In case of AVR system, we firstly introduce a $PIDND^2N^2$ controller designed for enhanced precision, stability, and responsiveness in voltage regulation. This configuration mitigates the limitations associated with conventional methods, promising superior control performance. Secondly, the b-AOA optimizer fine-tunes the parameters of our proposed control scheme, improving its overall performance and adaptability. Using the ZLG cost function [22], we target the minimization of dynamic response performance criteria, such as maximum overshoot, steady-state error, settling time, and rise time, thereby ensuring that the AVR system meets the most stringent performance requirements. Our work seeks to transcend theoretical innovation, anchoring itself in the practical applicability of power systems, where stability and reliability are non-negotiable. Through extensive simulations and rigorous experimentation, we aim to demonstrate the superiority of the b-AOA-based AVR system in comparison to existing control and optimization techniques. Our focus on stability, speed of response, robustness, and efficiency aligns with the motivations presented, making our work a substantial contribution to the field of power system control.

To validate the superiority of the proposed b-AOA approach, we conducted extensive comparative analyses, evaluating its performance against well-established control methodologies, such as the sine cosine algorithm (SCA)-based PID controller [23], whale optimization algorithm (WOA)-based PIDA controller [24], slime mould algorithm (SMA)-based FOPID controller [25], and particle swarm optimization (PSO)-based $PIDD^2$ controller [26]. The results unequivocally demonstrate that the b-AOA-based approach outshines its counterparts. It exhibits unmatched transient response characteristics, with the shortest rise time (0.033485 s) and settling time (0.050752 s) while eliminating overshoot. In contrast, other methods exhibit less favorable response characteristics. In terms of frequency response, the b-AOA approach consistently excels, showcasing robust stability, favorable gain margins, and a broader bandwidth.

To further assess the effectiveness of the proposed approach, we compared it with several other established controller approaches reported in the literature. These included the several recently reported control methods for the AVR system. These methods include a variety of controllers, each tuned using different optimization algorithms such as marine predators algorithm (MPA) based

Preprints (www.preprints.org) | NOT PEER-REVIEWED | Posted: 7 November 2023 doi:10.20944/preprints202311.0390.v1

FOPID [27], hybrid atom search particle swarm optimization (h-ASPSO) based PID [28], equilibrium optimizer (EO) based TIλDND2N2 based controller, reptile search algorithm (RSA) based FOPIDD2 [6], improved Runge-Kutta (iRUN) algorithm based PIDND2N2 [29], symbiotic organism search (SOS) algorithm-based PID-F [30], whale optimization algorithm (WOA) based 2DOF FOPI [31], Lévy flight-based RSA with local search ability (L-RSANM) based PID [32], chaotic black widow algorithm (ChBWO) based FOPID [15], genetic algorithm (GA) based fuzzy PID [33], sine-cosine algorithm (SCA) based FOPID with fractional order filter [34], hybrid simulated annealing–Manta ray foraging optimization (SA-MRFO) algorithm based PIDD2 [35], slime mould algorithm (SMA) based PID [14], gradient based optimization (GBO) based FOPID [36] and nonlinear SCA based sigmoid PID [37]. We evaluate their transient response performance to assess the effectiveness of the proposed approach. The results demonstrate the efficacy of the b-AOA-based PIDND^{2}N^2 controller in comparison to various state-of-the-art methods as it stands out with an impressive performance, suggesting the exceptional stability and responsiveness of the b-AOA-tuned controller.

These important results underscore the significance of our work, offering a superior solution for addressing the challenges in AVR control. It not only contributes to the advancement of power systems but also sets a new benchmark for stability, responsiveness, and reliability in this critical domain.

2. Overview of Arithmetic Optimization Algorithm

The arithmetic optimization algorithm (AOA) draws inspiration from arithmetic principles [5] to construct a versatile metaheuristic optimization technique. It initiates the optimization process by generating a set of randomized solutions represented as follows.

$$X = \begin{bmatrix} x_{1,1} & \cdots & \cdots & x_{1,j} & x_{1,n-1} & x_{1,n} \\ x_{2,1} & \cdots & \cdots & x_{2,j} & \cdots & x_{2,n} \\ \cdots & \cdots & \cdots & \cdots & \cdots & \cdots \\ \vdots & \vdots & \vdots & \vdots & \vdots & \vdots \\ x_{N-1,1} & \cdots & \cdots & x_{N-1,j} & \cdots & x_{N-1,n} \\ x_{N,1} & \cdots & \cdots & x_{N,j} & x_{N,n-1} & x_{N,n} \end{bmatrix} \quad (1)$$

Following this, the algorithm employs a function known as "Math Optimizer Accelerated" (MopA) to execute exploration and exploitation tasks. The MopA function is defined as:

$$MopA(t) = Min + t \times \left(\frac{Max - Min}{t_{max}}\right) \quad (2)$$

where t represents the current iteration, t_{max} denotes the maximum number of iterations, Min and Max represent the minimum and maximum values of the accelerated function. The exploration phase of the algorithm is carried out when $r_1 > MopA$, where r_1 is a randomly generated number. During exploration, the multiplication ($Mult$) and division (Div) operators are employed, defined as follows:

$$x_{i,j}(t+1) = \begin{cases} best(x_j) \times MopP \times \left(\left(UB_j - LB_j\right) \times \mu + LB_j\right), & \text{for } r_2 > 0.5 \\ best(x_j) \div (MopP + \epsilon) \times \left(\left(UB_j - LB_j\right) \times \mu + LB_j\right), & \text{for } r_2 < 0.5 \end{cases} \quad (3)$$

where $x_{i,j}(t)$ represents the j^{th} position of solution i at the current iteration, $x_i(t+1)$ denotes the solution of i in the next iteration, $best(x_j)$ signifies the best solution's j^{th} position obtained so far, ϵ is a small integer, μ is a control parameter that adjusts the search process, UB_j and LB_j respectively represent the upper and lower bounds of the j^{th} position. The "Math optimizer probability" function, denoted by MopP, is computed as follows, with α reflecting the exploitation accuracy through iterations.

$$MopP(t) = 1 - \frac{(t)^{1/\alpha}}{(t_{max})^{1/\alpha}} \quad (4)$$

The term r_2 is another random number utilized for position updates. The $Mult$ operator is employed for $r_2 > 0.5$, while the Div operator is used otherwise. Conversely, the exploitation phase

Preprints (www.preprints.org) | NOT PEER-REVIEWED | Posted: 7 November 2023 doi:10.20944/preprints202311.0390.v1

occurs when $r_1 < MopA$. In this stage, the addition (Add) and subtraction (Sub) operators are utilized, defined as.

$$x_{i,j}(t+1) = \begin{cases} best(x_j) + MopP \times \left((UB_j - LB_j) \times \mu + LB_j \right), & \text{for } r_3 > 0.5 \\ best(x_j) - MopP \times \left((UB_j - LB_j) \times \mu + LB_j \right), & \text{for } r_3 < 0.5 \end{cases} \quad (5)$$

Here, r_3 is a random number determining whether the Add or Sub operation is applied. Add operates when $r_3 > 0.5$, while Sub is used for $r_3 < 0.5$. Figure 1 presents a comprehensive flowchart of the AOA, depicting its intricate process.

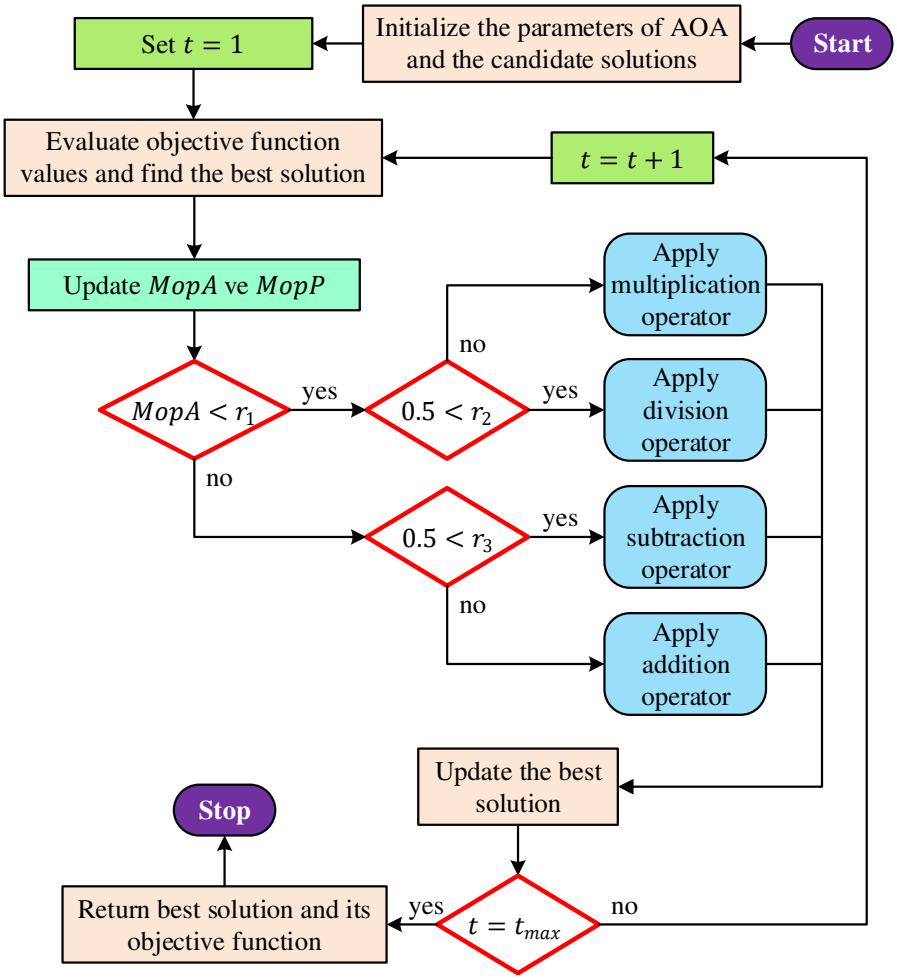

Figure 1. Flowchart of the original arithmetic optimization algorithm.

3. Balanced Arithmetic Optimization Algorithm

The balanced AOA (b-AOA) is an evolution of the pattern search (PS) [38] and the opposition-based learning (OBL) [39] schemes, designed to enhance both exploration and exploitation capabilities in the context of metaheuristic optimization. This section provides a step-by-step explanation of the b-AOA algorithm's development and its core components.

The PS scheme serves as the foundation for b-AOA. It is a derivative-free algorithm known for its exploitation capabilities [40]. PS starts with an initial point (X_0) defined by the user and proceeds by generating a mesh around this point, gradually updating the mesh as new points with lower objective function values are discovered. The process involves the following key steps:

- Exploration Stage: If a new point with a lower objective function value ($f(X_1) < f(X_0)$) is found (successful poll), it becomes the source point. The mesh size is then expanded by a factor of 2, creating new points for exploration.

Preprints (www.preprints.org) | NOT PEER-REVIEWED | Posted: 7 November 2023 doi:10.20944/preprints202311.0390.v1

- Exploitation Stage: When no new points with lower values are discovered, the mesh size is reduced by multiplying it by 0.5 (reduction factor). This contraction stage continues until the termination condition is met.

The detailed flowchart of the PS scheme is illustrated in Figure 2.

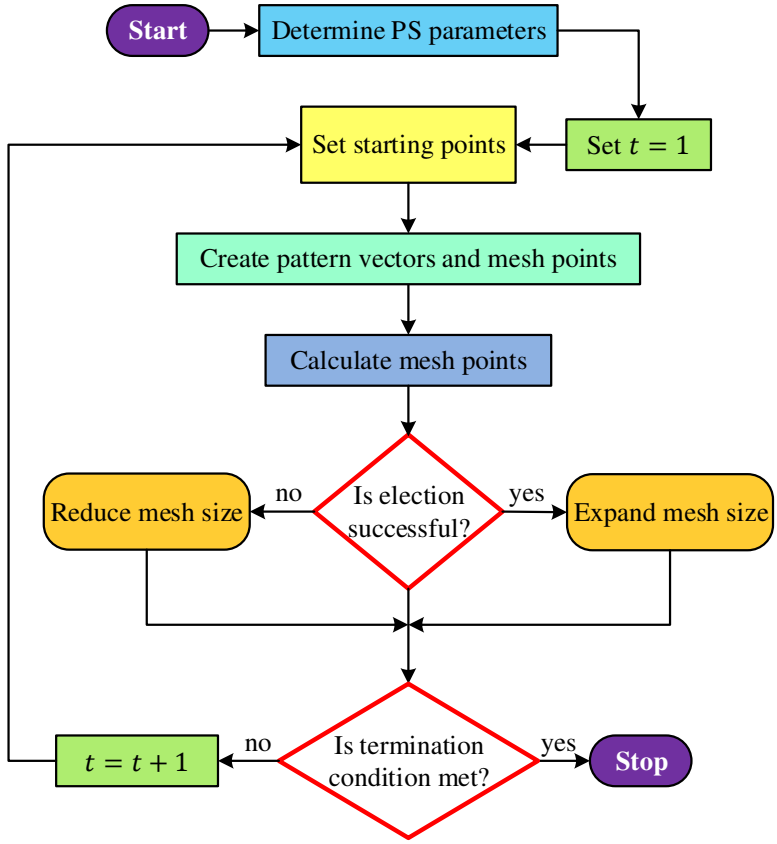

Figure 2. Flowchart of pattern search method.

The OBL scheme, introduced as a machine learning technique, enhances the performance of metaheuristic algorithms by considering both the current individuals and their opposites [39]. A special type of OBL mechanism known as elite OBL (EOBL) [41] focuses on the elite (best) individuals in combination with the current individuals. EOBL generates opposite solutions for the elite individuals, which are then evaluated for their fitness. The mathematical representation of the EOBL strategy is as follows:

- Elite candidate solution: $X = \langle x_1, x_2 \dots, x_k \rangle$ with k decision variables.
- Elite opposition-based solution $X^o = \langle x_1^o, x_2^o \dots, x_k^o \rangle$ where $x_i^o = \delta(da_i + db_i) - x_i$ and δ is a parameter within the range (0, 1) controlling the opposition magnitude.
- Dynamic boundaries: $da_i = min(x_i), db_i = max(x_i)$
- To ensure that opposite decision variables stay within the boundaries $[Lb_i, Ub_i]$, the following rule is applied: $x_i^o = rand(Lb_i, Ub_i)$, if $x_i^o < Lb_i$ or $x_i^o > Ub_i$.

The working principle of the OBL mechanism is depicted in Figure 3.

Preprints (www.preprints.org) | NOT PEER-REVIEWED | Posted: 7 November 2023 doi:10.20944/preprints202311.0390.v1

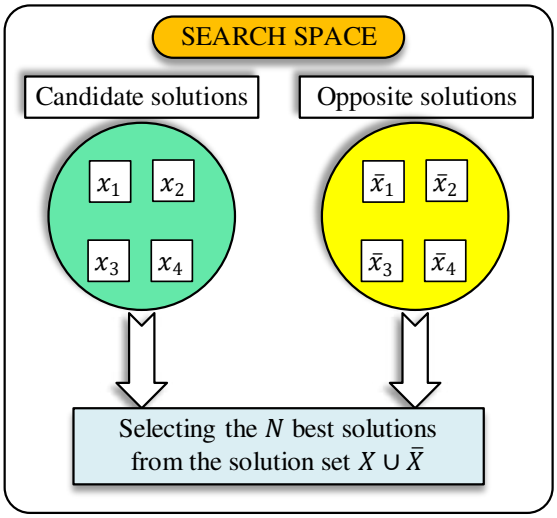

Figure 3. Working principle of OBL mechanism.

The b-AOA algorithm integrates the EOBL and the PS schemes to achieve a balanced approach with improved exploration and exploitation capabilities. Figure 4 provides an overview of the b-AOA algorithm's operation. As depicted in the figure:

- The algorithm commences with the original AOA and generates the best solution.
- The EOBL scheme is introduced to produce N best solutions.
- The PS scheme takes over to enhance exploitation, running a total of 5 times with 100×D iterations, where D represents the problem's dimension size.

The parameters for the b-AOA algorithm, derived from extensive simulations, include:

- PS scheme parameters: initial mesh size = 1, mesh expansion factor = 2, mesh contraction factor = 0.5, and all tolerances = 10^{-6}.
- AOA algorithm parameters: sensitive parameter $\alpha = 5$, control parameter $\mu = 0.4975$, $Min = 0.2$, $Max = 1$.

Preprints (www.preprints.org) | NOT PEER-REVIEWED | Posted: 7 November 2023 doi:10.20944/preprints202311.0390.v1

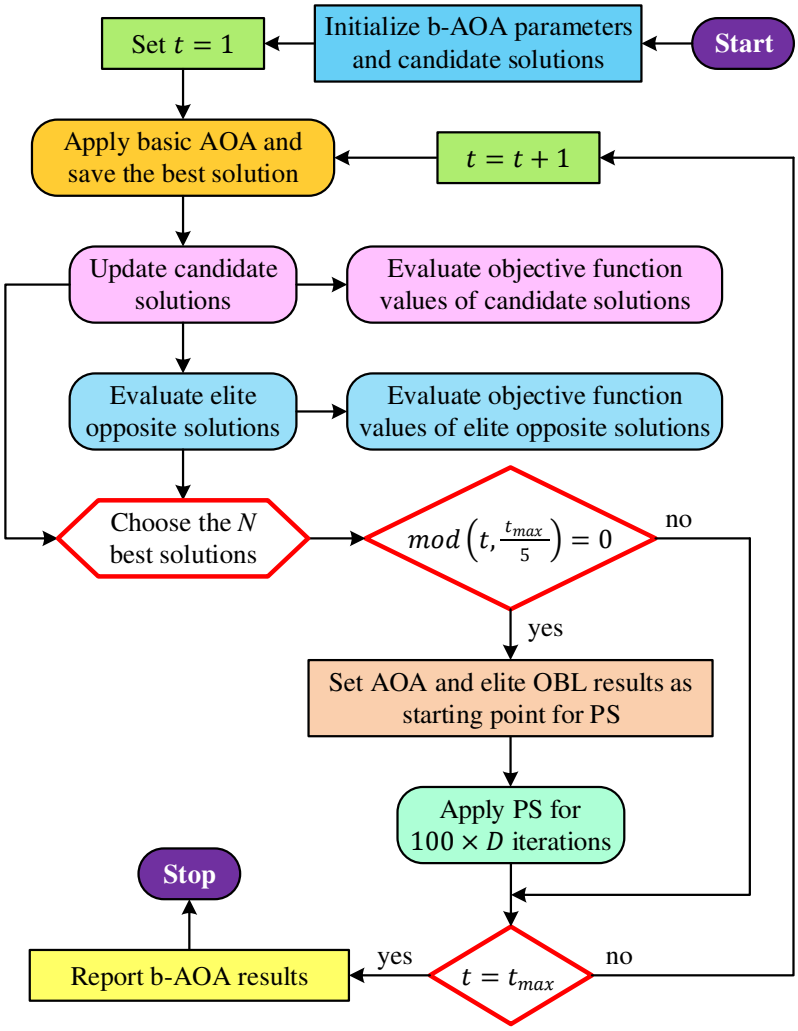

Figure 4. Flowchart of proposed b-AOA algorithm.

4. Adopted Test functions

$$Func_1(x) = \sum_{i=1}^{Dim} x_i^2 \tag{6}$$

$$Func_2(x) = \sum_{i=1}^{Dim} |x_i| + \prod_{i=1}^{Dim} |x_i| \tag{7}$$

$$Func_3(x) = \sum_{i=1}^{Dim} \left(\sum_{j=1}^{i} x_j \right)^2 \tag{8}$$

$$Func_4(x) = \max_i \{|x_i|, 1 \le i \le Dim\} \tag{9}$$

$$Func_5(x) = \sum_{i=1}^{Dim-1} (100(x_{i+1} - x_i^2)^2 + (x_i - 1)^2) \tag{10}$$

4.1. Unimodal Benchmark Functions

Preprints (www.preprints.org) | NOT PEER-REVIEWED | Posted: 7 November 2023 doi:10.20944/preprints202311.0390.v1

$$Func_6(x) = \sum_{i=1}^{Dim} (x_i + 0.5)^2 \tag{11}$$

$$Func_7(x) = \sum_{i=1}^{Dim} ix_i^4 + random[0,1) \tag{12}$$

In this section, we introduce a set of unimodal benchmark functions that have been adopted for our study. These benchmark functions are commonly used in the field of optimization to evaluate the performance of optimization algorithms and to compare their effectiveness. The following unimodal benchmark functions have been selected for our analysis: Sphere, Schwefel 2.2, Schwefel 1.2, Schwefel 2.21, Rosenbrock, Step and Quartic. The mathematical equations defining these benchmark functions are respectively provided in the following equations.

In addition to the mathematical expressions for these benchmark functions, we have compiled essential properties and information related to each function in Table 1. This table provides details on the dimensionality of each function, the evaluation interval, and the global minimum values. These properties are crucial for understanding the characteristics of each benchmark function and for conducting a comprehensive analysis of the optimization algorithms' performance.

Table 1. Properties of the adopted unimodal benchmark functions.

Name	Function	Dimension	Evaluation interval	Global minimum
Sphere	$Func_1(x)$	30	$[-100, 100]^{Dim}$	0
Schwefel 2.2	$Func_2(x)$	30	$[-10, 10]^{Dim}$	0
Schwefel 1.2	$Func_3(x)$	30	$[-100, 100]^{Dim}$	0
Schwefel 2.21	$Func_4(x)$	30	$[-100, 100]^{Dim}$	0
Rosenbrock	$Func_5(x)$	30	$[-30, 30]^{Dim}$	0
Step	$Func_6(x)$	30	$[-100, 100]^{Dim}$	0
Quartic	$Func_7(x)$	30	$[-1.28, 1.28]^{Dim}$	0

4.2. Multimodal Benchmark Functions

In this section, we introduce a collection of multimodal benchmark functions that have been selected for our research. Multimodal functions are essential for assessing the capability of optimization algorithms to handle complex, non-convex search spaces, where multiple local optima exist. The following multimodal benchmark functions have been chosen for our study: Schwefel, Rastrigin, Ackley, Griewank, Penalized and Penalized2. The mathematical equations representing these benchmark functions are respectively provided in the following equations.

$$Func_8(x) = -\sum_{i=1}^{Dim} \left(x_i \sin\left(\sqrt{|x_i|}\right)\right) \tag{13}$$

$$Func_9(x) = \sum_{i=1}^{Dim} [10 + x_i^2 - 10\cos(2\pi x_i)] \tag{14}$$

$$Func_{10}(x) = 20 + e - 20exp\left(-0.2\sqrt{\frac{1}{Dim}\sum_{i=1}^{Dim} x_i^2}\right) - exp\left(\frac{1}{Dim}\sum_{i=1}^{Dim}\cos(2\pi x_i)\right) \tag{15}$$

$$Func_{11}(x) = \sum_{i=1}^{Dim} \frac{x_i^2}{4000} - \prod_{i=1}^{Dim} \cos\left(\frac{x_i}{\sqrt{i}}\right) + 1 \tag{16}$$

Preprints (www.preprints.org) | NOT PEER-REVIEWED | Posted: 7 November 2023 doi:10.20944/preprints202311.0390.v1

$$Func_{12}(x) = \frac{\pi}{Dim}\left\{10\sin^2(\pi y_1) + \sum_{i=1}^{Dim-1}(y_i-1)^2[1+10\sin^2(\pi y_{i+1})] + (y_{Dim}-1)^2\right\} + \sum_{i=1}^{Dim} u(x_i,10,100,4) \quad (17)$$

$$Func_{13}(x) = 0.1\left\{\sin^2(3\pi x_1) + \sum_{i=1}^{Dim-1}(x_i-1)^2[1+\sin^2(3\pi x_{i+1})] + (x_{Dim}-1)^2[1+\sin^2(2\pi x_{Dim})]\right\} + \sum_{i=1}^{Dim} u(x_i,5,100,4) \quad (18)$$

Moreover, to facilitate a comprehensive understanding of these benchmark functions, we have compiled vital properties and information for each function in Table 2. This table presents information on the dimensionality of each function, the evaluation interval, and the global minimum values. These properties are pivotal for comprehending the characteristics of each benchmark function and for the subsequent analysis of optimization algorithms in handling multimodal search spaces.

Table 2. Properties of the adopted multimodal benchmark functions.

Name	Function	Dimension	Evaluation interval	Global minimum
Schwefel	$Func_8(x)$	30	$[-500,500]^{Dim}$	−1.2569E+04
Rastrigin	$Func_9(x)$	30	$[-5.12,5.12]^{Dim}$	0
Ackley	$Func_{10}(x)$	30	$[-32,32]^{Dim}$	0
Griewank	$Func_{11}(x)$	30	$[-600,600]^{Dim}$	0
Penalized	$Func_{12}(x)$	30	$[-50,50]^{Dim}$	0
Penalized2	$Func_{13}(x)$	30	$[-50,50]^{Dim}$	0

4.3. Fixed-dimensional Multimodal Test Functions

This section introduces a collection of fixed-dimensional multimodal test functions, which are indispensable for evaluating the performance of optimization algorithms in solving problems with known characteristics. These benchmark functions are specifically selected for their fixed-dimensional nature, making them suitable for comparing and benchmarking various optimization techniques. The following fixed-dimensional multimodal test functions have been included in our study: Foxholes, Kowalik, Six-Hump Camel, Branin, Goldstein-Price, Hartman 3, Hartman 6, Shekel 5, Shekel 7 and Shekel 10. The mathematical equations describing these fixed-dimensional multimodal test functions can respectively be found in the following equations.

$$Func_{14}(x) = \frac{1}{\left(\frac{1}{500} + \sum_{j=1}^{25}\frac{1}{j+\sum_{i=1}^{2}(x_i-a_{ij})^6}\right)} \quad (19)$$

$$Func_{15}(x) = \sum_{i=1}^{11}\left[a_i - \frac{x_1(b_i^2+b_i x_2)}{b_i^2+b_i x_3+x_4}\right]^2 \quad (20)$$

$$Func_{16}(x) = 4x_1^2 - 2.1x_1^4 + \frac{1}{3}x_1^6 + x_1x_2 - 4x_2^2 + 4x_2^4 \quad (21)$$

$$Func_{17}(x) = 10\left(1-\frac{1}{8\pi}\right)\cos x_1 + 10 + \left(x_2 - \frac{5.1}{4\pi^2}x_1^2 + \frac{5}{\pi}x_1 - 6\right)^2 \quad (22)$$

Preprints (www.preprints.org) | NOT PEER-REVIEWED | Posted: 7 November 2023 doi:10.20944/preprints202311.0390.v1

$$Func_{18}(x) = [30 + (2x_1 - 3x_2)^2 \times (18 - 32x_1 + 12x_1^2 + 48x_2 - 36x_1x_2 + 27x_2^2)] \times [1 + (x_1 + x_2 + 1)^2(19 - 14x_1 + 3x_1^2 - 14x_2 + 6x_1x_2 + 3x_2^2)] \quad (23)$$

$$Func_{19}(x) = -\sum_{i=1}^{4} c_i exp\left(-\sum_{j=1}^{3} a_{ij}(x_j - p_{ij})^2\right) \quad (24)$$

$$Func_{20}(x) = -\sum_{i=1}^{4} c_i exp\left(-\sum_{j=1}^{6} a_{ij}(x_j - p_{ij})^2\right) \quad (25)$$

$$Func_{21}(x) = -\sum_{i=1}^{5} \frac{1}{(X - a_i)(X - a_i)^T + c_i} \quad (26)$$

$$Func_{22}(x) = -\sum_{i=1}^{7} \frac{1}{(X - a_i)(X - a_i)^T + c_i} \quad (27)$$

$$Func_{23}(x) = -\sum_{i=1}^{10} \frac{1}{(X - a_i)(X - a_i)^T + c_i} \quad (28)$$

To further enhance the understanding of these benchmark functions, essential properties and information for each function are summarized in Table 3. This table provides key details such as the dimensionality of each function, the evaluation interval, and the global minimum values, enabling a comprehensive evaluation and comparison of optimization algorithms for fixed-dimensional search spaces.

Table 3. Properties of the adopted fixed-dimensional multimodal benchmark functions.

Name	Function	Dimension	Evaluation interval	Global minimum
Foxholes	$Func_{14}(x)$	2	$[-65.536, 65.536]^{Dim}$	0.998
Kowalik	$Func_{15}(x)$	4	$[-5, 5]^{Dim}$	3.0749E−04
Six-Hump Camel	$Func_{16}(x)$	2	$[-5, 5]^{Dim}$	−1.0316
Branin	$Func_{17}(x)$	2	$[-5, 10] \times [0, 15]$	0.39789
Goldstein-Price	$Func_{18}(x)$	2	$[-2, 2]^{Dim}$	3
Hartman 3	$Func_{19}(x)$	3	$[0, 1]^{Dim}$	−3.8628
Hartman 6	$Func_{20}(x)$	6	$[0, 1]^{Dim}$	−3.322
Shekel 5	$Func_{21}(x)$	4	$[0, 10]^{Dim}$	−10.1532
Shekel 7	$Func_{22}(x)$	4	$[0, 10]^{Dim}$	−10.4029
Shekel 10	$Func_{23}(x)$	4	$[0, 10]^{Dim}$	−10.5364

5. Statistical performance of the b-AOA on Test Functions

5.1. Compared Algorithms

In our study, we have evaluated the performance of several optimization algorithms against proposed b-AOA by comparing their effectiveness in solving the benchmark functions. The algorithms considered for comparison include the following: original AOA [5], sine-cosine algorithm (SCA) [19], weighted mean of vectors (INFO) algorithm [20] and marine predators algorithm (MPA) [21].

For each of these algorithms, we conducted 30 independent runs to ensure robust and comprehensive assessment. By executing multiple independent runs, we aimed to account for the inherent variability in optimization processes and obtain reliable results.

Preprints (www.preprints.org) | NOT PEER-REVIEWED | Posted: 7 November 2023 doi:10.20944/preprints202311.0390.v1

Table 4 presents key properties and control parameters associated with the compared algorithms. These properties include the population size, total iteration number, and values of other control parameters specific to each algorithm.

Table 4. Properties of the compared algorithms (population size, total iteration number, values of other control parameters).

Algorithm	Population size	Total iteration number	Values of other control parameters
b-AOA	30	500	$\alpha = 5,\ \mu = 0.4975,\ Min = 0.2,\ Max = 1,$ $initial\ mesh\ size = 1,\ mesh\ expansion\ factor = 2,$ $mesh\ contraction\ factor = 0.5,$ $all\ tolerances = 10^{-6}$
AOA [5]	30	500	$\alpha = 5,\ \mu = 0.4975,\ Min = 0.2,\ Max = 1$
SCA [19]	30	500	$A = 2$
INFO [20]	30	500	$c = 2,\ d = 4$
MPA [21]	30	500	$FADs = 0.2,\ P = 0.5$

5.2. Statistical Results Obtained from Unimodal Benchmark Functions

In this section, we present the comparative statistical results obtained from the evaluation of unimodal benchmark functions using various optimization algorithms. The analysis is based on the mean, standard deviation, best, and worst performance of each algorithm across the unimodal benchmark functions. Table 5 summarizes these results. Upon examining the data in Table 5, we can draw several important observations:

- Sphere Function: The b-AOA algorithm demonstrates superior performance, achieving a mean error of zero across multiple runs. In contrast, other algorithms exhibit varying degrees of error, with AOA achieving the lowest mean error but still far from the precision of b-AOA.
- Schwefel 2.2 Function: Similar to the Sphere function, b-AOA outperforms other algorithms by achieving a mean error close to zero. The other algorithms, in contrast, exhibit significant errors.
- Schwefel 1.2 and Schwefel 2.21 Functions: In both cases, b-AOA once again stands out with extremely low mean errors, indicating its effectiveness in solving these functions. The other algorithms show larger mean errors.
- Rosenbrock Function: While the b-AOA algorithm exhibits a higher mean error compared to some other algorithms, it still achieves competitive results, and its worst-case performance is better than some other algorithms. It is important to note that the Rosenbrock function is known for its challenging optimization landscape.
- Step Function: b-AOA demonstrates exceptional performance with a mean error close to zero. The other algorithms exhibit more significant errors, making b-AOA the most effective choice for this function.
- Quartic Function: Once again, b-AOA shows strong performance, with a mean error significantly lower than other algorithms. It is evident that b-AOA consistently performs exceptionally well across multiple unimodal benchmark functions.

In summary, the results obtained from the unimodal benchmark functions highlight the efficacy of the proposed b-AOA algorithm. It consistently achieves mean errors close to zero, demonstrating its capability to find accurate solutions. While some other algorithms perform well on specific functions, b-AOA stands out as a robust choice across various unimodal benchmark functions, making it a promising optimization algorithm for solving such problems.

Table 5. Comparative statistical results obtained from unimodal benchmark functions.

Function	Algorithm	Mean	Standard Deviation	Best	Worst
$Func_1(x)$	b-AOA	0	0	0	0

Preprints (www.preprints.org) | NOT PEER-REVIEWED | Posted: 7 November 2023 doi:10.20944/preprints202311.0390.v1

	AOA	0.00029656	0.0011413	3.9226E−38	0.0060134
	SCA	16.537	36.426	9.5633E−06	175.47
	INFO	1.0185E−53	4.997E−54	3.3545E−55	2.0178E−53
	MPA	4.0116E−23	6.3963E−23	3.6461E−25	2.7727E−22
	b-AOA	8.5996E−241	0	4.333E−320	2.2954E−239
	AOA	2.8674E−186	0	9.6235E−296	8.6022E−185
$Func_2(x)$	SCA	0.021241	0.031567	0.00013767	0.13042
	INFO	1.0943E−26	3.6605E−27	4.7283E−27	1.9892E−26
	MPA	2.6444E−13	2.8514E−13	8.2406E−15	1.2622E−12
	b-AOA	0	0	0	0
	AOA	1.6011	3.3816	1.3815E−07	16.177
$Func_3(x)$	SCA	8640.8	4939.5	1709.5	20103
	INFO	1.4606E−50	1.1602E−50	8.6654E−52	3.9712E−50
	MPA	9.9612E−05	0.00022346	7.2658E−09	0.001186
	b-AOA	9.0422E−244	0	1.2808E−253	2.6479E−242
	AOA	0.15416	0.094877	0.014632	0.36318
$Func_4(x)$	SCA	37.033	13.087	12.166	61.964
	INFO	2.1028E−27	1.4215E−27	3.5852E−28	7.4954E−27
	MPA	2.7542E−09	1.5152E−09	3.1553E−10	6.0257E−09
	b-AOA	0.61615	1.8814	3.0737E−09	6.3967
	AOA	28.693	0.27549	27.902	29.18
$Func_5(x)$	SCA	1.3673E+05	3.2682E+05	107.54	1175700
	INFO	22.585	0.51711	21.298	23.462
	MPA	25.268	0.45451	24.487	26.042
	b-AOA	2.4395E−12	9.2009E−13	1.086E−12	5.8521E−12
	AOA	3.7524	0.33331	3.0561	4.4582
$Func_6(x)$	SCA	14.254	13.542	4.7191	55.025
	INFO	1.2654E−08	3.7987E−08	3.9266E−11	2.07E−07
	MPA	4.1868E−08	2.2575E−08	1.3296E−08	1.2965E−07
	b-AOA	3.629E−05	2.8489E−05	6.8524E−07	0.00010771
	AOA	9.4896E−05	7.1313E−05	2.0672E−06	0.00029718
$Func_7(x)$	SCA	0.099158	0.090509	0.0085847	0.44986
	INFO	0.0015937	0.0012634	0.00017227	0.0049221
	MPA	0.0013495	0.00060352	0.00041966	0.0026601

5.3. Statistical Results Obtained from Multimodal Benchmark Functions

In this section, we analyze the comparative statistical results obtained from the evaluation of multimodal benchmark functions using various optimization algorithms. The statistical metrics considered include the mean, standard deviation, best, and worst performance for each algorithm across the multimodal benchmark functions. Table 6 summarizes these results. Upon examining the data in Table 6, several key observations can be made:

- Schwefel Function: The b-AOA algorithm exhibits a mean error of -12536, which is notably closer to the global minimum of this multimodal function. It also achieves the lowest standard deviation, indicating a high level of consistency in its performance. The worst-case result is still very competitive, showing the effectiveness of b-AOA in solving the Schwefel function.
- Rastrigin Function: Interestingly, for the Rastrigin function, all algorithms, including b-AOA, achieve a mean error of zero. While b-AOA doesn't stand out in this case, it demonstrates a comparable performance to other algorithms.
- Ackley Function: For the Ackley function, b-AOA achieves a mean error close to zero, indicating its effectiveness in minimizing the function. The standard deviation is also very low, demonstrating consistent results.

Preprints (www.preprints.org) | NOT PEER-REVIEWED | Posted: 7 November 2023 doi:10.20944/preprints202311.0390.v1

- Griewank Function: Similar to the Rastrigin function, all algorithms, including b-AOA, achieve a mean error of zero. While b-AOA performs equally well in terms of mean error, its consistency is reflected in a lower standard deviation.
- Penalized and Penalized2 Functions: The b-AOA algorithm outperforms other algorithms in minimizing both the Penalized and Penalized2 functions, as indicated by the lower mean error. Its consistent performance is highlighted by the low standard deviation, making it a robust choice for solving these multimodal functions.

In summary, the results obtained from the multimodal benchmark functions emphasize the efficacy of the proposed b-AOA algorithm. It not only achieves competitive mean errors but also demonstrates remarkable consistency in its performance, as reflected by the low standard deviations. This consistency is essential for solving complex multimodal functions where the optimization landscape can be highly challenging. The b-AOA algorithm's ability to approach the global minimum and its robustness make it a strong candidate for addressing multimodal optimization problems.

Table 6. Comparative statistical results obtained from multimodal benchmark functions.

Function	Algorithm	Mean	Standard Deviation	Best	Worst
	b-AOA	−12536	172.87	−12569	−11623
	AOA	−7980.7	446.84	−9196.5	−7230.3
$Func_8(x)$	SCA	−3848.4	286.86	−4371	−3283.7
	INFO	−8630.7	700.38	−9763.3	−7101.2
	MPA	−8736.9	438.15	−9687.9	−7946.9
	b-AOA	0	0	0	0
	AOA	0	0	0	0
$Func_9(x)$	SCA	29.308	30.189	0.13996	122.46
	INFO	0	0	0	0
	MPA	0	0	0	0
	b-AOA	8.8818E−16	0	8.8818E−16	8.8818E−16
	AOA	8.8818E−16	0	8.8818E−16	8.8818E−16
$Func_{10}(x)$	SCA	14.208	8.3212	0.043401	20.382
	INFO	8.8818E−16	0	8.8818E−16	8.8818E−16
	MPA	1.7196E−12	1.1519E−12	2.7045E−13	5.8482E−12
	b-AOA	0	0	0	0
	AOA	194.12	65.896	72.408	323.52
$Func_{11}(x)$	SCA	0.84569	0.41164	0.23545	1.9083
	INFO	0	0	0	0
	MPA	0	0	0	0
	b-AOA	2.1943E−13	1.5539E−13	5.0331E−14	6.0379E−13
	AOA	0.29154	0.053809	0.14538	0.43947
$Func_{12}(x)$	SCA	52428	1.5261E+05	1.0947	614430
	INFO	1.4456E−09	2.8117E−09	5.3463E−12	1.1459E−08
	MPA	0.00014286	0.0005059	2.4157E−09	0.0023059
	b-AOA	3.1668E−12	2.4141E−12	7.6907E−13	9.0849E−12
	AOA	2.4484	0.16915	2.1217	2.8078
$Func_{13}(x)$	SCA	1.0872E+05	2.7869E+05	2.2042	1305400
	INFO	0.063752	0.14273	3.2034E−10	0.69157
	MPA	0.012215	0.036876	2.8969E−08	0.19763

5.4. Statistical Results Obtained from Fixed-dimensional Multimodal Benchmark Functions

This section provides an analysis of the comparative statistical results obtained from the evaluation of fixed-dimensional multimodal benchmark functions using various optimization

Preprints (www.preprints.org) | NOT PEER-REVIEWED | Posted: 7 November 2023 doi:10.20944/preprints202311.0390.v1

algorithms. The data in Table 7 presents the mean, standard deviation, best, and worst performance of each algorithm for these functions. Key insights drawn from the data in Table 7 include:

- Foxholes Function: The b-AOA algorithm stands out as it achieves a mean error of 0.998, which is very close to the global minimum of this function. Moreover, it demonstrates an extremely low standard deviation, indicating remarkable consistency. The best and worst-case performance metrics further underscore its effectiveness in solving the Foxholes function.
- Kowalik Function: The b-AOA algorithm once again excels, achieving a mean error of 0.00030749, which is impressively close to the global minimum. The standard deviation is nearly zero, highlighting its exceptional consistency. In contrast, other algorithms exhibit higher mean errors and standard deviations.
- Six-Hump Camel Function: b-AOA performs exceptionally well, achieving a mean error close to the global minimum and an almost negligible standard deviation. This indicates its strong capability to solve the Six-Hump Camel function effectively.
- Branin Function: The b-AOA algorithm continues to demonstrate outstanding performance with a mean error of 0.39789, very close to the global minimum. It also exhibits an absence of standard deviation, showcasing the consistency of its results.
- Goldstein-Price Function: The b-AOA algorithm delivers optimal performance by achieving a mean error of 3. This not only aligns with the global minimum but is also consistent without any standard deviation. This makes it a standout performer for the Goldstein-Price function.
- Hartman 3, Hartman 6, Shekel 5, Shekel 7, Shekel 10 Functions: Across all of these functions, the b-AOA algorithm consistently achieves a mean error close to the global minimum, with negligible standard deviations. This underscores its efficacy in solving these fixed-dimensional multimodal benchmark functions.

In summary, the results obtained from the fixed-dimensional multimodal benchmark functions highlight the efficacy of the proposed b-AOA algorithm. It consistently delivers mean errors close to the global minimum and demonstrates exceptional consistency with minimal standard deviations. This performance makes b-AOA a robust choice for solving a wide range of fixed-dimensional multimodal functions, showing its potential as a versatile optimization algorithm.

Table 7. Comparative statistical results obtained from fixed-dimensional multimodal benchmark functions.

Function	Algorithm	Mean	Standard Deviation	Best	Worst
	b-AOA	0.998	1.5701E−17	0.998	0.998
	AOA	8.3696	3.2389	0.998	12.671
$Func_{14}(x)$	SCA	1.795	0.9859	0.998	2.9821
	INFO	2.1111	2.5903	0.998	10.763
	MPA	0.998	1.515E−16	0.998	0.998
	b-AOA	0.00030749	1.4923E−15	0.00030749	0.00030749
	AOA	0.015417	0.025604	0.00037189	0.11249
$Func_{15}(x)$	SCA	0.0010661	0.00037002	0.0005829	0.0015477
	INFO	0.0024352	0.0060863	0.00030749	0.020363
	MPA	0.00030749	4.3122E−15	0.00030749	0.00030749
	b-AOA	−1.0316	1.9902E−16	−1.0316	−1.0316
	AOA	−1.0316	6.0816E−07	−1.0316	−1.0316
$Func_{16}(x)$	SCA	−1.0316	3.7905E−05	−1.0316	−1.0315
	INFO	−1.0316	6.5843E−16	−1.0316	−1.0316
	MPA	−1.0316	4.4024E−16	−1.0316	−1.0316
	b-AOA	0.39789	0	0.39789	0.39789
	AOA	0.40987	0.009864	0.39844	0.43767
$Func_{17}(x)$	SCA	0.40026	0.0023543	0.39797	0.40949
	INFO	0.39789	0	0.39789	0.39789
	MPA	0.39789	9.5078E−15	0.39789	0.39789

Preprints (www.preprints.org) | NOT PEER-REVIEWED | Posted: 7 November 2023 doi:10.20944/preprints202311.0390.v1

	b-AOA	3	0	3	3
	AOA	6.6	9.3351	3	30
$Func_{18}(x)$	SCA	3	5.4359E−05	3	3.0002
	INFO	3	8.6883E−16	3	3
	MPA	3	2.1709E−15	3	3
	b-AOA	−3.8628	2.4116E−15	−3.8628	−3.8628
	AOA	−3.8523	0.0038518	−3.8593	−3.842
$Func_{19}(x)$	SCA	−3.8547	0.0024361	−3.861	−3.8495
	INFO	−3.8628	2.6823E−15	−3.8628	−3.8628
	MPA	−3.8628	2.4945E−15	−3.8628	−3.8628
	b-AOA	−3.322	2.1608E−13	−3.322	−3.322
	AOA	−3.0471	0.091025	−3.1762	−2.8234
$Func_{20}(x)$	SCA	−2.8784	0.34163	−3.1199	−1.6747
	INFO	−3.2784	0.058273	−3.322	−3.2031
	MPA	−3.322	1.7554E−11	−3.322	−3.322
	b-AOA	−10.153	7.6605E−13	−10.153	−10.153
	AOA	−3.5023	1.1997	−6.0307	−1.8035
$Func_{21}(x)$	SCA	−2.6202	2.0715	−7.8686	−0.49728
	INFO	−9.1039	2.4723	−10.153	−2.6305
	MPA	−10.153	4.1471E−11	−10.153	−10.153
	b-AOA	−10.403	1.1144E−12	−10.403	−10.403
	AOA	−3.5619	1.2118	−6.8762	−1.4002
$Func_{22}(x)$	SCA	−3.2023	1.8303	−5.9956	−0.52105
	INFO	−9.0488	2.7774	−10.403	−2.7659
	MPA	−10.403	5.9857E−11	−10.403	−10.403
	b-AOA	−10.536	3.2315E−12	−10.536	−10.536
	AOA	−3.8733	1.6156	−6.5892	−1.5825
$Func_{23}(x)$	SCA	−3.7421	1.7935	−6.1434	−0.94135
	INFO	−9.0039	3.151	−10.536	−2.4217
	MPA	−10.536	2.5368E−11	−10.536	−10.536

6. Automatic Voltage regulator System

6.1. Components of AVR System and Its Modeling

The AVR system comprises four key main components: the exciter, generator, sensor, and amplifier, each of which plays a crucial vital role in the system's performance. Figure 5 illustrates the schematic diagram of a typical AVR system, providing an overview of its structural components.

Preprints (www.preprints.org) | NOT PEER-REVIEWED | Posted: 7 November 2023 doi:10.20944/preprints202311.0390.v1

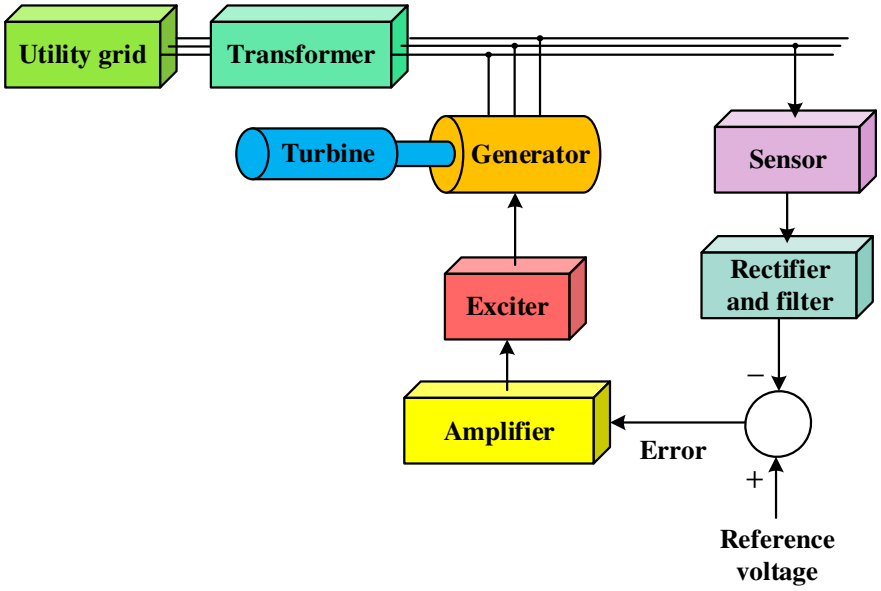

Figure 5. Schematic diagram of a typical AVR system.

To model the AVR system effectively, it is essential to define the transfer functions and constraints for each of these components. The transfer function for the amplifier is given by:

$$G_{amp} = \frac{K_{amp}}{1 + sT_{amp}} \tag{29}$$

which is subjected to constraints of $10 \leq K_{amp} \leq 40$ ve $0.02 \leq T_{amp} \leq 0.1$. The transfer function for the exciter is represented as:

$$G_{exc} = \frac{K_{exc}}{1 + sT_{exc}} \tag{30}$$

with constraints of $1 \leq K_{exc} \leq 10$ ve $0.4 \leq T_{exc} \leq 1$. The generator's transfer function is defined as:

$$G_{gen} = \frac{K_{gen}}{1 + sT_{gen}} \tag{31}$$

which has constraints of $0.7 \leq K_{gen} \leq 1$ ve $1 \leq T_{gen} \leq 2$. The sensor's transfer function is presented as:

$$H_{sen} = \frac{K_{sen}}{1 + sT_{sen}} \tag{32}$$

which is constrained by $0.9 \leq K_{sen} \leq 1.1$ ve $0.001 \leq T_{sen} \leq 0.06$. To facilitate a fair comparison with literature reports, specific parameter values of $K_{amp} = 10$, $T_{amp} = 0.1\ s$, $K_{exc} = 1$, $T_{exc} = 0.4\ s$, $K_{gen} = 1$, $T_{gen} = 1\ s$, $K_{sen} = 1$ ve $T_{sen} = 0.01\ s$ [23–26] are employed in this study. By applying these parameter values, the transfer function for an uncontrolled AVR system can be derived as follows.

$$\begin{aligned} T_{no-control}(s) &= \frac{G_{amp}(s) \times G_{exc}(s) \times G_{gen}(s)}{1 + G_{amp}(s) \times G_{exc}(s) \times G_{gen}(s) \times H_{sen}(s)} \\ &= \frac{0.1s + 10}{0.0004s^4 + 0.0454s^3 + 0.555s^2 + 1.51s + 11} \end{aligned} \tag{33}$$

An uncontrolled AVR system, with its main components, is illustrated in Figure 6.

Preprints (www.preprints.org) | NOT PEER-REVIEWED | Posted: 7 November 2023 doi:10.20944/preprints202311.0390.v1

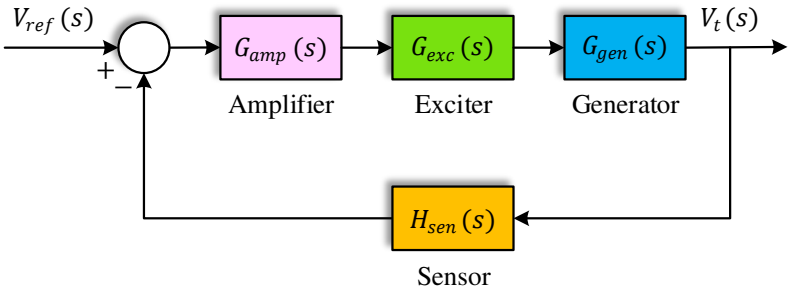

Figure 6. An Uncontrolled AVR system.

6.2. Pole-zero Map of an Uncontrolled AVR System

The pole-zero map of the uncontrolled AVR system is depicted in Figure 7. The system's poles are located at -99.9712, -12.4892, and -0.5198 ± 4.6642i, while it possesses only one zero at -100. The system exhibits a very low damping ratio (11.1%) for complex poles, indicating the necessity for enhancing the performance of the uncontrolled system.

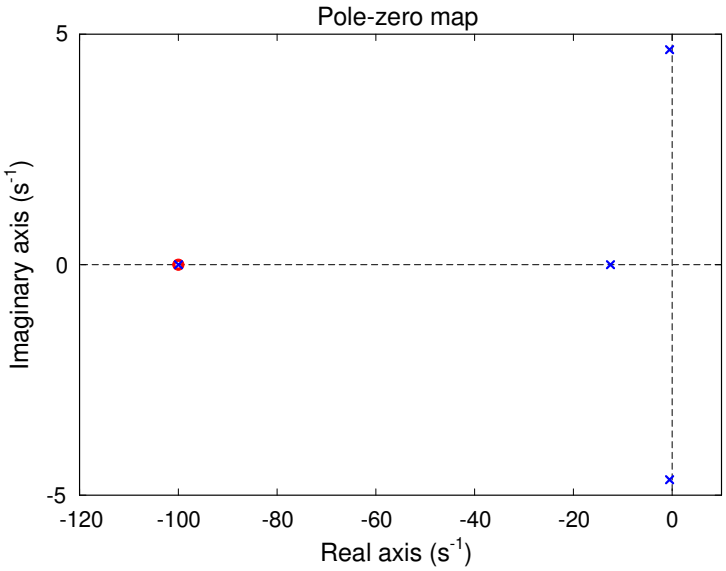

Figure 7. Pole-zero map of uncontrolled AVR system.

6.3. Time Domain Response of an Uncontrolled AVR System

The unit step response of the uncontrolled AVR system is illustrated in Figure 8. The relevant system exhibits a maximum overshoot of 65.7226%, a rise time of 0.2607 seconds, a settling time of 6.9865 seconds, and a peak time of 0.7522 seconds. These values are considerably large for a power system, and the proposed control approach aims to enhance the performance of the AVR system. Therefore, the proposed control strategy aims to significantly improve the performance of the AVR system.

Preprints (www.preprints.org) | NOT PEER-REVIEWED | Posted: 7 November 2023 doi:10.20944/preprints202311.0390.v1

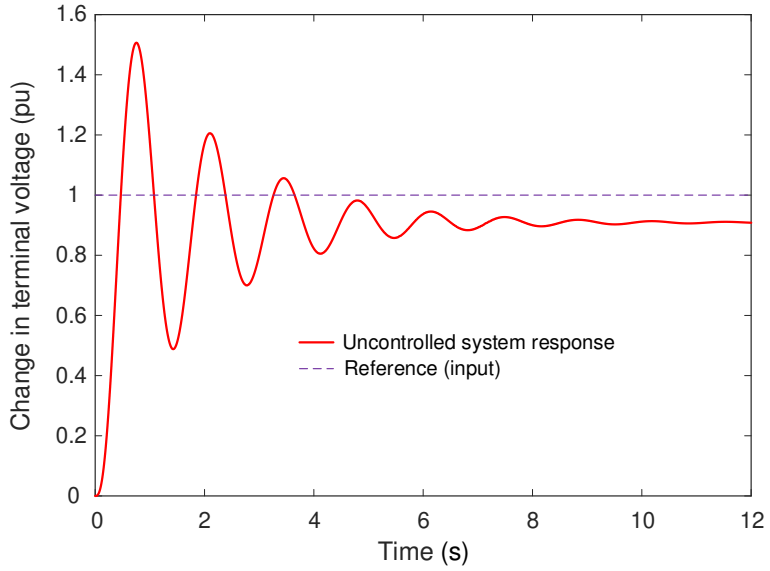

Figure 8. Step response of the uncontrolled AVR system.

6.4. Open-loop Frequency Response of an Uncontrolled AVR System

Figure 9 displays the Bode plot of the uncontrolled open-loop AVR system. This system exhibits a gain margin of 4.6176 dB, a phase margin of 16.1028 degrees, and a bandwidth of 6.9454 rad/s. Just as with the time response criteria, it is evident that the frequency response criteria also require improvement through an effective control approach.

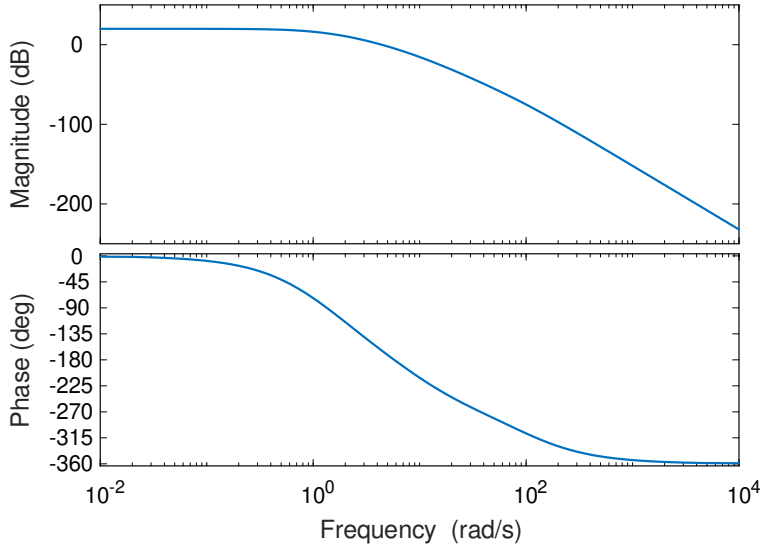

Figure 9. Open loop Bode plot of the uncontrolled AVR system.

7. The Proposed Novel Design method for AVR System

7.1. Reported Controller Types and PIDND²N² controller

In the context of the AVR system, several controller types have been reported and applied. These controllers play a critical role in regulating and stabilizing the system's voltage. The transfer functions of some of the most commonly reported controllers, including PID, PIDA, FOPID, PIDD², and PIDND²N², are respectively provided in equations (34) to (38) [9,42].

$$C_{PID}(s) = K_p + \frac{K_i}{s} + K_d s \tag{34}$$

Preprints (www.preprints.org) | NOT PEER-REVIEWED | Posted: 7 November 2023 doi:10.20944/preprints202311.0390.v1

$$C_{PIDA}(s) = \frac{K_a s^3 + K_d s^2 + K_p s + K_i}{s^3 + \alpha s^2 + \beta s} \tag{35}$$

$$C_{FOPID}(s) = K_p + \frac{K_i}{s^\lambda} + K_d s^\mu \tag{36}$$

$$C_{PIDD^2}(s) = K_p + \frac{K_i}{s} + K_{d1} s + K_{d2} s^2 \tag{37}$$

$$C_{PIDND^2N^2}(s) = K_p + \frac{K_i}{s} + K_{d1} \frac{n_1 s}{s + n_1} + K_{d2} \frac{(n_2 s)^2}{(s + n_2)^2} \tag{38}$$

In the specific context of the AVR system, these controller types have been employed to regulate voltage. For this study, the PIDND²N² controller was selected due to its effectiveness in achieving the desired control objectives. A visual representation of the PIDND2N2 controller can be found in Figure 10.

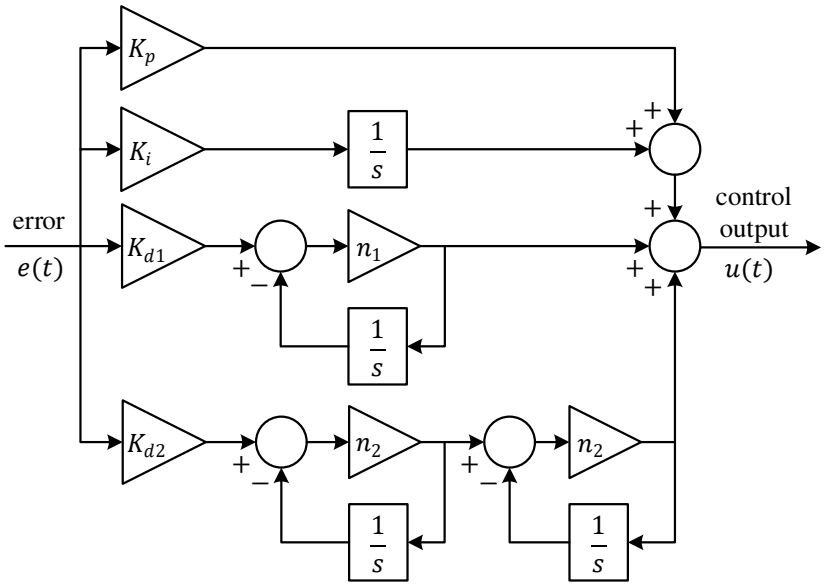

Figure 10. Block diagram of PIDND²N² controller.

7.2. Objective Function

In the literature, it is feasible to encounter commonly used error-based objective functions of F_{IAE} (Integral of the Absolute Error), F_{ISE} (Integral of the Square of the Error), F_{ITAE} (Integral of Time-weighted Absolute Error), and F_{ITSE} (Integral of Time-weighted Square of the Error). Their definitions are provided in the following equations [43].

$$F_{IAE} = \int_0^\infty |e(t)| \cdot dt \tag{39}$$

$$F_{ISE} = \int_0^\infty (e(t))^2 \cdot dt \tag{40}$$

$$F_{ITAE} = \int_0^\infty t \cdot |e(t)| \cdot dt \tag{41}$$

Preprints (www.preprints.org) | NOT PEER-REVIEWED | Posted: 7 November 2023 doi:10.20944/preprints202311.0390.v1

$$F_{ITSE} = \int_0^{\infty} t \cdot (e(t))^2 \cdot dt \tag{42}$$

In equations (39) - (42), the term $e(t)$ represents the error signal, which, for the AVR system, is defined as $e(t) = V_t - V_{ref}$ where V_t is terminal voltage and V_{ref} Is the reference voltage. Additionally, the F_{ZLG} objective function, which utilizes time response performance criteria, is widely employed in the literature. In this study, the latter one has been preferred which is given by the following equation [22].

$$F_{ZLG} = (1 - \theta) \cdot (MP + ES) + \theta \cdot (ST - RT) \tag{43}$$

In equation (46), MP denotes the maximum overshoot, ES stands for the steady-state error, ST represents the settling time, and RT signifies the rise time. The parameter θ in the equation serves as a weighting factor and is set to $e^{-1} = 0.3679$ in this study.

7.3. Integration of the Algorithm to PIDND²N² Controlled AVR System

Table 8 lists the lower and upper boundary values used for controller parameters when applying the proposed b-AOA algorithm to the PIDND²N² controller. These values are utilized during the optimization process to determine the range within which parameter values should be sought.

Table 8. Boundaries for PIDND²N² Controller parameters.

Bound	K_p	K_i	K_{d1}	K_{d2}	n_1	n_2
Lower	0.001	0.001	0.001	0.001	50	50
Upper	5	5	5	5	2000	2000

Figure 11 illustrates a block diagram depicting the application of the proposed b-AOA algorithm, along with the PIDND²N² controller and the ZLG objective function, to the AVR system. As depicted in the figure, the best values for the relevant controller parameters are calculated based on the minimization of the ZLG objective function.

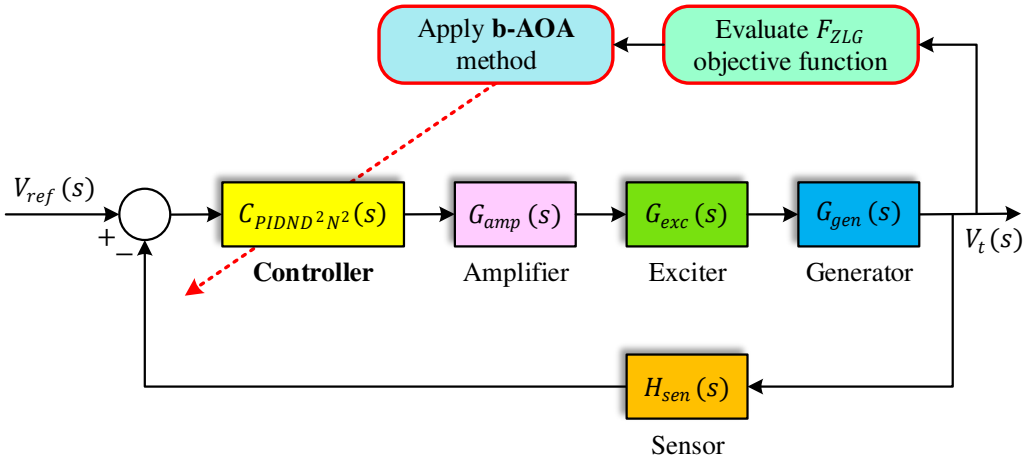

Figure 11. The block diagram of the implementation of the proposed approach to AVR system.

8. Simulation Results and Discussion

8.1. Statistical Performance of b-AOA and AOA Methods for AVR System

In the optimization of the AVR system, the b-AOA and AOA algorithms were executed 30 times. A population size of 30 and a maximum iteration count of 50 were chosen for minimizing the objective function. The statistical results obtained from all runs are presented in Table 9. As observed in the table, all statistical metrics for optimizing the F_ZLG objective function favor the b-AOA

Preprints (www.preprints.org) | NOT PEER-REVIEWED | Posted: 7 November 2023 doi:10.20944/preprints202311.0390.v1

algorithm, indicating its superior performance. These results additionally confirm the statistical stability of the b-AOA algorithm.

Table 9. Statistical performance of b-AOA and original AOA for AVR system.

Algorithm	Mean	Standard Deviation	Best	Worst
b-AOA	0.0065138	9.3497E−05	0.0063522	0.0067022
AOA	0.0078863	0.00012395	0.0076825	0.0081212

8.2. Obtained Best Controller Parameters and Transfer Functions of the Optimized System

In this section, we discuss the results regarding the best controller parameters and the corresponding transfer functions of the optimized system. Figure 12 provides the convergence curve, illustrating the progress of the b-AOA and the original AOA algorithms in minimizing the objective function. Notably, it shows that the b-AOA outperforms the original AOA by achieving the lowest objective function value through iterations.

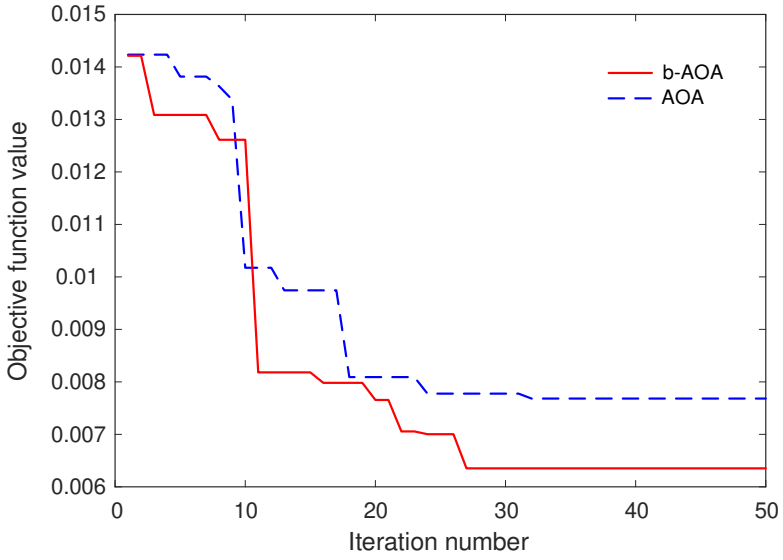

Figure 12. Convergence curve for b-AOA and original AOA

Table 10 presents the optimal parameters of the PIDND²N² controller, obtained using both the b-AOA and the original AOA algorithms.

Table 10. Optimal parameters of PIDND²N² controller obtained via b-AOA and original AOA algorithms

Optimized by	K_p	K_i	K_{d1}	K_{d2}	n_1	n_2
b-AOA	4.8723	2.0240	1.8094	0.15049	1595.2	1971.2
AOA	3.9448	2.1188	1.6757	0.13014	1544.2	871.72

Using those values would yield the following transfer functions of the optimized systems for original AOA and proposed b-AOA algorithms.

$$T_{AOA-PIDND^2N^2}(s) = \frac{1.015e04s^5+1.674e07s^4+1.77e09s^3+2.026e10s^2+4.661e10s+2.486e10}{0.0004s^8+1.36s^7+1531s^6+6.279e05s^5+5.621e07s^4+2.229e09s^3+2.157e10s^2+4.754e10s+2.486e10} \quad (44)$$

$$T_{b-AOA-PIDND^2N^2}(s) = \frac{5.876e04s^5+1.003e08s^4+1.057e10s^3+1.157e11s^2+3.035e11s+1.255e11}{0.0004s^8+2.26s^7+4322s^6+2.944e06s^5+2.929e08s^4+1.29e10s^3+1.22e11s^2+3.084e11s+1.255e11} \quad (45)$$

8.3. Stability of the Proposed Design Method

In this section, we analyze the stability of the proposed design method by evaluating the step response and open-loop frequency response of the b-AOA and AOA-tuned PIDND²N² controllers.

Preprints (www.preprints.org) | NOT PEER-REVIEWED | Posted: 7 November 2023 doi:10.20944/preprints202311.0390.v1

Figure 13 and Table 11 present the transient response performance metrics for the b-AOA and AOA-tuned PIDND²N² controllers. The step response of both controllers is observed concerning the change in the terminal voltage. As illustrated in Figure 13, the b-AOA-tuned PIDND2N2 controller exhibits a faster rise time and settling time with zero overshoot compared to the AOA-tuned PIDND²N² controller. This implies that the b-AOA tuned system reaches the desired state more rapidly without oscillations, demonstrating its superior stability in the time domain. The numerical results from Table 11 confirm these visual observations.

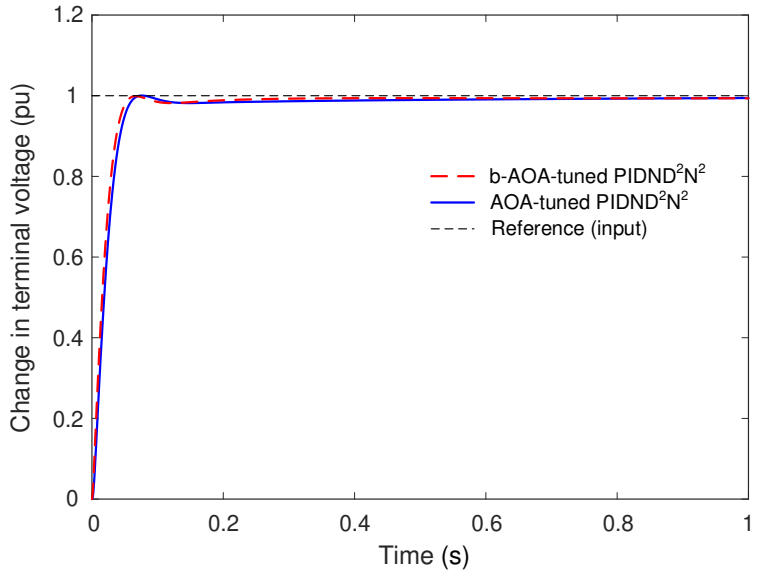

Figure 13. Step response of b-AOA and AOA-tuned PIDND²N² controllers for the change in the terminal voltage.

Table 11. Transient response performance metrics for b-AOA and AOA-tuned PIDND²N² controllers.

Design method	Rise time (s)	Settling time (s)	Overshoot (%)
b-AOA-tuned PIDND²N²	**0.033485**	**0.050752**	**0**
AOA-tuned PIDND²N²	0.037393	0.057523	0.043859

Figure 14 and Table 12 present the open loop Bode diagrams and frequency response performance metrics for the controllers. In the frequency domain, the b-AOA-tuned PIDND²N² controller showcases a higher phase margin, greater gain margin, and a wider bandwidth compared to the AOA-tuned PIDND²N² controller. These results signify that the b-AOA-based controller maintains better stability and frequency response characteristics, making it superior in terms of overall system stability.

Preprints (www.preprints.org) | NOT PEER-REVIEWED | Posted: 7 November 2023 doi:10.20944/preprints202311.0390.v1

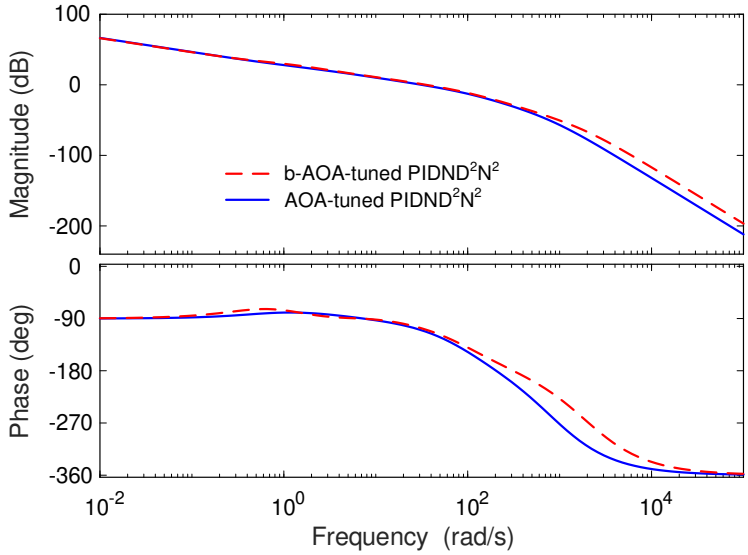

Figure 14. Open loop Bode diagrams for b-AOA and AOA-tuned PIDND²N² controllers

Table 12. Frequency response performance metrics for b-AOA and AOA-tuned PIDND²N² controllers.

Design method	Phase margin (°)	Gain margin (dB)	Bandwidth (rad/s)
b-AOA-tuned PIDND²N²	70.797	28.888	64.820
AOA-tuned PIDND²N²	69.810	23.368	57.819

8.4. Compared Algorithms and Respective Transfer Functions

In this section, we provide a comparative analysis of well-known methods in the literature, which employ different types of controllers. The controller types used in these approaches are as follows: sine cosine algorithm (SCA)-based PID controller [23], whale optimization algorithm (WOA)-based PIDA controller [24], slime mould algorithm (SMA)-based FOPID controller [25], and particle swarm optimization (PSO)-based PIDD² controller [26].

The parameters for the SCA-based PID controller [23] are as follows: $K_p = 0.9826$, $K_i = 0.8337$ and $K_d = 0.4982$. The transfer function of the closed-loop AVR system using this approach is given by the following equation.

$$T_{SCA-PID}(s) = \frac{0.04982s^3 + 5.08s^2 + 9.909s + 8.337}{0.0004s^5 + 0.0454s^4 + 0.555s^3 + 6.492s^2 + 10.83s + 8.337} \quad (46)$$

The parameters for the WOA-based PIDA controller [24] are as follows: $K_p = 777.401$, $K_i = 397.741$, $K_d = 500.652$, $K_a = 103.02$, $\alpha = 550.118$ and $\beta = 915.041$. The transfer function of the closed-loop AVR system using this approach is given by the following equation.

$$T_{WOA-PIDA}(s) = \frac{10.3s^4 + 1080s^3 + 5084s^2 + 7814s + 3977}{0.0004s^7 + 0.2654s^6 + 25.9s^5 + 348.4s^4 + 2370s^3 + 6938s^2 + 8689s + 3977} \quad (47)$$

The parameters for the SMA-based FOPID controller [25] are as follows: $K_p = 2.2554$, $K_i = 1.2586$, $K_d = 0.6472$, $\lambda = 1.0274$ and $\mu = 1.1877$. The transfer function of the closed-loop AVR system using this approach is given by the following equation.

$$T_{SMA-FOPID}(s) = \frac{0.06472s^{3.2151} + 6.472s^{2.2151} + 0.22554s^{2.0274} + 22.554s^{1.0274} + 0.12586s + 12.586}{0.0004s^{5.0274} + 0.0454s^{4.0274} + 0.555s^{3.0274} + 6.472s^{2.2151} + 1.51s^{2.0274} + 23.554s^{1.0274} + 12} \quad (48)$$

Preprints (www.preprints.org) | NOT PEER-REVIEWED | Posted: 7 November 2023 doi:10.20944/preprints202311.0390.v1

The parameters for the PSO-based PIDD² controller [26] are as follows: $K_p = 2.7784$, $K_i = 1.8521$, $K_{d1} = 0.9997$ and $K_{d2} = 0.07394$. The transfer function of the closed-loop AVR system using this approach is given by the following equation.

$$T_{PSO-PIDD^2}(s) = \frac{0.007394s^4 + 0.8394s^3 + 10.27s^2 + 27.97s + 18.52}{0.0004s^5 + 0.0454s^4 + 1.294s^3 + 11.51s^2 + 28.78s + 18.52} \quad (49)$$

These equations define the transfer functions of the AVR systems under the influence of different control methods. The following subsections provide a comparative analysis of these methods based on various performance criteria.

8.5. Comparative Transient Response Analysis

Figure 15 displays the comparative step response of different control approaches for the AVR system. This figure visually represents the transient response of various control methods and provides insights into their performance. The step response graph shows how each method reacts to a change in the terminal voltage.

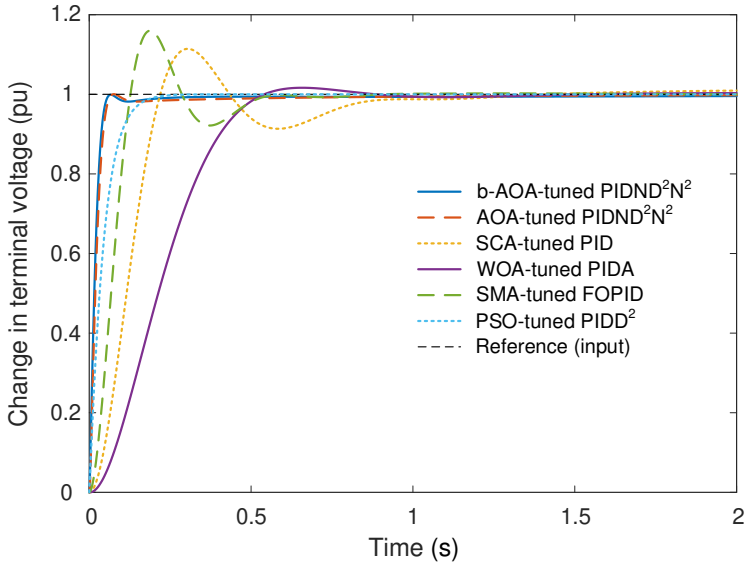

Figure 15. Comparative step response of different control approaches for AVR system

Table 13 complements the visual representation by providing numerical values for the transient response metrics of different control approaches. These metrics include the rise time, settling time, and overshoot, which are essential indicators of the system's dynamic behavior.

Table 13. Comparative numerical values for transient response of different control approaches.

Design method	Rise time (s)	Settling time (s)	Overshoot (%)
b-AOA-tuned PIDND²N²	**0.033485**	**0.050752**	**0**
AOA-tuned PIDND²N²	0.037393	0.057523	0.043859
SCA-tuned PID [23]	0.1472	0.84133	11.425
WOA-tuned PIDA [24]	0.32772	0.49543	1.6483
SMA-tuned FOPID [25]	0.087541	0.4979	15.998
PSO-tuned PIDD² [26]	0.092935	0.16347	0.0025797

Upon analyzing both the figure and the table, it becomes evident that the b-AOA-tuned PIDND²N² controller excels in achieving a superior transient response compared to other control approaches. It exhibits the shortest rise time (0.033485 s) and settling time (0.050752 s) while completely eliminating overshoot. In contrast, the other control methods, including AOA, SCA-tuned PID, WOA-tuned PIDA, SMA-tuned FOPID, and PSO-tuned PIDD², exhibit longer rise and settling

Preprints (www.preprints.org) | NOT PEER-REVIEWED | Posted: 7 November 2023 doi:10.20944/preprints202311.0390.v1

times and, in some cases, significant overshoot. These results emphasize the superiority of the b-AOA-based control approach in providing a faster and more stable transient response, which is crucial for maintaining the AVR system's stability and performance during dynamic voltage changes.

8.6. Comparative Frequency Response Analysis

Figure 16 provides a comparative view of Bode diagrams for different control approaches applied to the AVR system. These diagrams illustrate the frequency response characteristics of each control method, offering insights into how they perform across a range of frequencies.

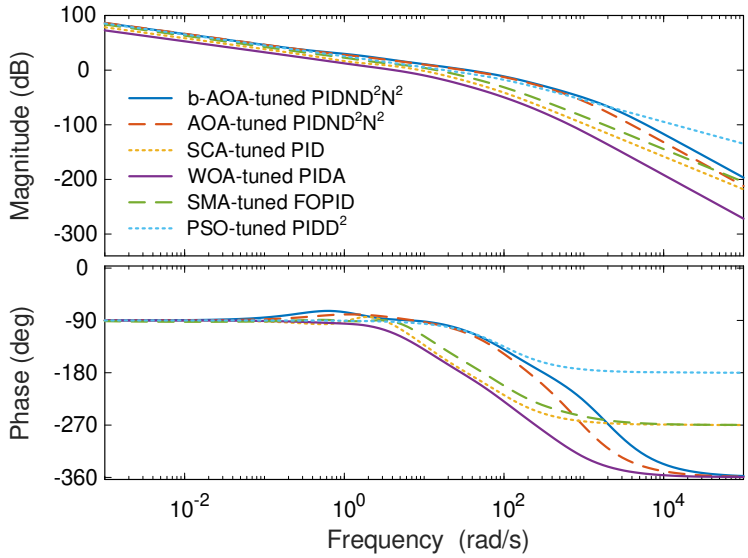

Figure 16. Comparative Bode diagrams of different control approaches for AVR system

Table 14 complements the visual representation with numerical values that quantify the frequency response metrics for each control approach. These metrics include the phase margin, gain margin, and bandwidth, which are crucial indicators of the system's stability and ability to handle varying frequencies.

Table 14. Comparative numerical values for frequency response of different control approaches.

Design method	Phase margin (°)	Gain margin (dB)	Bandwidth (rad/s)
b-AOA-tuned PIDND²N²	70.797	28.888	64.820
AOA-tuned PIDND²N²	69.810	23.368	57.819
SCA-tuned PID [33]	52.596	20.300	14.821
WOA-tuned PIDA [34]	67.671	26.123	6.7076
SMA-tuned FOPID [35]	49.142	20.193	23.914
PSO-tuned PIDD² [36]	79.638	Infinite	23.503

Upon analyzing both the figure and the table, it is clear that the b-AOA-tuned PIDND²N² controller stands out as the superior choice for frequency response analysis. It exhibits the highest phase margin (70.797°), indicating robust stability and the most favorable gain margin (28.888 dB) among all the methods, ensuring ample room for gain adjustments without instability. Moreover, it possesses the widest bandwidth (64.82 rad/s), signifying a faster system response to frequency variations. In contrast, the other control approaches, including AOA-tuned PIDND²N², SCA-tuned PID, WOA-tuned PIDA, SMA-tuned FOPID, and PSO-tuned PIDD², generally display lower phase margins, lower gain margins, and narrower bandwidths. The b-AOA-based controller, on the other hand, excels in maintaining system stability across a broad frequency range and offers improved performance for handling dynamic frequency changes. These results underscore the superiority of the b-AOA-tuned PIDND²N² controller in providing robust and responsive frequency characteristics,

Preprints (www.preprints.org) | NOT PEER-REVIEWED | Posted: 7 November 2023 doi:10.20944/preprints202311.0390.v1

which are vital for the stable and efficient operation of the AVR system under various operating conditions.

8.7. Comparisons with the Reported Recent Works

In this section, we compare the proposed PIDND2N2 controller tuned with b-AOA to several recently reported control methods for the AVR system. These methods include a variety of controllers, each tuned using different optimization algorithms such as marine predators algorithm (MPA) based FOPID [27], hybrid atom search particle swarm optimization (h-ASPSO) based PID [28], equilibrium optimizer (EO) based TIλDND2N2 based controller, reptile search algorithm (RSA) based FOPIDD2 [6], improved Runge-Kutta (iRUN) algorithm based PIDND2N2 [29], symbiotic organism search (SOS) algorithm-based PID-F [30], whale optimization algorithm (WOA) based 2DOF FOPI [31], Lévy flight-based RSA with local search ability (L-RSANM) based PID [32], chaotic black widow algorithm (ChBWO) based FOPID [15], genetic algorithm (GA) based fuzzy PID [33], sine-cosine algorithm (SCA) based FOPID with fractional order filter [34], hybrid simulated annealing–Manta ray foraging optimization (SA-MRFO) algorithm based PIDD2 [35], slime mould algorithm (SMA) based PID [14], gradient based optimization (GBO) based FOPID [36] and nonlinear SCA based sigmoid PID [37].

We evaluate their transient response performance to assess the effectiveness of the proposed approach. Table 15 provides a comprehensive overview of the transient response metrics, including rise time, settling time, and overshoot, for the proposed approach and other recent methods. The results demonstrate the efficacy of the b-AOA-based PIDND^{2}N^2 controller in comparison to various state-of-the-art methods as it stands out with an impressive performance, featuring a remarkably low rise time (0.033485s), a fast settling time (0.050752s), and zero overshoot. This suggests the exceptional stability and responsiveness of the b-AOA-tuned controller. Therefore, the table clearly illustrates the effectiveness of the proposed b-AOA-based PIDND^{2}N^2 controller in achieving rapid responses and maintaining stable performance, as evidenced by its minimal overshoot. It consistently outperforms or rivals the other methods in the evaluation, reinforcing its superiority for the AVR system's transient response.

Table 15. Transient response performance of the proposed approach with respect to recently reported other efficient methods.

Ref.	Year	Used controller type	Tuning method	Rise time (s)	Settling time (s)	Overshoot (%)
Proposed		**PIDND^{2}N^2**	**b-AOA**	**0.033485**	**0.050752**	**0**
[27]	2023	FOPID	MPA	0.0833	0.1106	0.55
[28]		PID	h-ASPSO	0.3097	0.4679	1.2476
[44]		TIλDND^{2}N^2	EO	0.03752	0.0596	0.4128
[6]		FOPIDD^2	RSA	0.0487	0.0806	0
[29]		PIDND^{2}N^2	iRUN	0.0399	0.0626	0
[30]	2022	PID-F	SOS	0.267	0.371	0.007
[31]		2DOF fractional-order PI	WOA	1.12	1.74	1.17
[32]		PID	L-RSANM	0.3076	0.4669	0.9582
[15]		FOPID	ChBWO	0.1103	0.169	1.1838
[33]		Fuzzy PID	GA	0.1857	0.2963	1.0407
[34]		FOPID with fractional filter	SCA	0.1230	0.1670	0.1262
[35]	2021	PIDD^2	SA-MRFO	0.0535	0.0798	0.7562
[14]		PID	SMA	0.3149	0.4817	0.6071
[36]		FOPID	GBO	0.0885	0.653	11.3
[37]		Sigmoid PID	NSCA	0.498	0.579	2.2

9. Conclusion and Future Works

In this study, we have introduced a novel approach to enhance the control of AVR in power systems. By uniting a PIDND²N² controller with the novel b-AOA, we aimed to address the limitations associated with conventional methods. The introduction of the PIDND²N² controller offers enhanced precision, stability, and responsiveness in voltage regulation. This innovative configuration mitigates the shortcomings of existing approaches, promising superior control performance. The b-AOA optimizer, meticulously fine-tuned with the integration of PS and EOBL strategies into original AOA in order to demonstrate exceptional performance. The assessment on 23 benchmark functions show that it consistently achieves accurate solutions, exhibits robustness in addressing various optimization problems, and showcases remarkable potential for a wide range of applications. Extensive comparative analyses reveal the superiority of the proposed approach in transient response characteristics. The b-AOA-based AVR control approach excels in rise time, settling time, and overshoot, outperforming other methods. It also ensures robust stability with favorable gain margins and a broader bandwidth, offering improved performance for handling dynamic frequency changes. The results of our work set a new benchmark for AVR control, advancing stability, responsiveness, and reliability in power systems.

Future work in this domain may focus on several aspects. Further refinement of the b-AOA optimization framework, exploring additional optimization problems, and evaluating its applicability to diverse domains are promising directions. Investigating the practical implementation of the proposed control scheme in real-world power systems and conducting extensive field testing would provide valuable insights. In addition, the AVR system can be considered as an important field of study in which it can play a critical role in the realization of the efficient voltage regulation in smart grids. Additionally, the integration of emerging technologies, such as machine learning and artificial intelligence, into AVR control systems may offer opportunities for further enhancement. The quest for more efficient, stable, and responsive AVR systems remains a vibrant field of research with potential breakthroughs on the horizon.

Author Contributions: All authors contributed equally. All authors have read and agreed to the published version of the manuscript.

Funding: This research received no external funding.

Data Availability Statement: All produced data are available within the manuscript.

Conflicts of Interest: The authors declare no conflict of interest.

References

1. Saat, S.; Ghazali, M.R.; Ahmad, M.A.; Mustapha, N.M.Z.A.; Tumari, M.Z.M. An Implementation of Brain Emotional Learning Based Intelligent Controller for AVR System. In Proceedings of the 2023 IEEE International Conference on Automatic Control and Intelligent Systems (I2CACIS); IEEE, June 17 2023; pp. 60–64.
2. Bhookya, J.; Jatoth, R.K. Optimal FOPID/PID Controller Parameters Tuning for the AVR System Based on Sine–Cosine-Algorithm. *Evol Intell* **2019**, *12*, 725–733, doi:10.1007/s12065-019-00290-x.
3. Micev, M.; Ćalasan, M.; Oliva, D. Fractional Order PID Controller Design for an AVR System Using Chaotic Yellow Saddle Goatfish Algorithm. *Mathematics* **2020**, *8*, 1182, doi:10.3390/math8071182.
4. Izci, D.; Ekinci, S.; Mirjalili, S. Optimal PID plus Second-Order Derivative Controller Design for AVR System Using a Modified Runge Kutta Optimizer and Bode's Ideal Reference Model. *Int J Dyn Control* **2023**, *11*, 1247–1264, doi:10.1007/s40435-022-01046-9.
5. Abualigah, L.; Diabat, A.; Mirjalili, S.; Abd Elaziz, M.; Gandomi, A.H. The Arithmetic Optimization Algorithm. *Comput Methods Appl Mech Eng* **2021**, *376*, 113609, doi:10.1016/j.cma.2020.113609.
6. Can, Ö.; Andiç, C.; Ekinci, S.; Izci, D. Enhancing Transient Response Performance of Automatic Voltage Regulator System by Using a Novel Control Design Strategy. *Electrical Engineering* **2023**, *105*, 1993–2005, doi:10.1007/s00202-023-01777-8.
7. Mok, R.; Ahmad, M.A. Fast and Optimal Tuning of Fractional Order PID Controller for AVR System Based on Memorizable-Smoothed Functional Algorithm. *Engineering Science and Technology, an International Journal* **2022**, *35*, 101264, doi:10.1016/j.jestch.2022.101264.

8. Ćalasan, M.; Micev, M.; Djurovic, Ž.; Mageed, H.M.A. Artificial Ecosystem-Based Optimization for Optimal Tuning of Robust PID Controllers in AVR Systems with Limited Value of Excitation Voltage. *The International Journal of Electrical Engineering & Education* **2020**, 002072092094060, doi:10.1177/0020720920940605.
9. Izci, D.; Ekinci, S.; Mirjalili, S.; Abualigah, L. An Intelligent Tuning Scheme with a Master/Slave Approach for Efficient Control of the Automatic Voltage Regulator. *Neural Comput Appl* **2023**, *35*, 19099–19115, doi:10.1007/s00521-023-08740-5.
10. Demirören, A.; Hekimoğlu, B.; Ekinci, S.; Kaya, S. Artificial Electric Field Algorithm for Determining Controller Parameters in AVR System. In Proceedings of the 2019 International Artificial Intelligence and Data Processing Symposium (IDAP); 2019; pp. 1–7.
11. Ekinci, S.; Can, Ö.; Izci, D. Controller Design for Automatic Voltage Regulator System Using Modified Opposition-Based Weighted Mean of Vectors Algorithm. *International Journal of Modelling and Simulation* **2023**, 1–18, doi:10.1080/02286203.2023.2274254.
12. Izci, D.; Rizk-Allah, R.M.; Snášel, V.; Ekinci, S.; Hashim, F.A.; Abualigah, L. A Novel Control Scheme for Automatic Voltage Regulator Using Novel Modified Artificial Rabbits Optimizer. *e-Prime - Advances in Electrical Engineering, Electronics and Energy* **2023**, *6*, 100325, doi:10.1016/j.prime.2023.100325.
13. Mohamadwasel, N.B. Rider Optimization Algorithm Implemented on the AVR Control System Using MATLAB with FOPID. *IOP Conf Ser Mater Sci Eng* **2020**, *928*, 032017, doi:10.1088/1757-899X/928/3/032017.
14. Izci, D.; Ekinci, S. Comparative Performance Analysis of Slime Mould Algorithm For Efficient Design of Proportional–Integral–Derivative Controller. *Electrica* **2021**, *21*, 151–159, doi:10.5152/electrica.2021.20077.
15. Munagala, V.K.; Jatoth, R.K. Improved Fractional PIλDμ Controller for AVR System Using Chaotic Black Widow Algorithm. *Computers & Electrical Engineering* **2022**, *97*, 107600, doi:https://doi.org/10.1016/j.compeleceng.2021.107600.
16. Alghamdi, S.; Sindi, H.F.; Rawa, M.; Alhussainy, A.A.; Calasan, M.; Micev, M.; Ali, Z.M.; Abdel Aleem, S.H.E. Optimal PID Controllers for AVR Systems Using Hybrid Simulated Annealing and Gorilla Troops Optimization. *Fractal and Fractional* **2022**, *6*, 682, doi:10.3390/fractalfract6110682.
17. Koessler, E.; Almomani, A. Hybrid Particle Swarm Optimization and Pattern Search Algorithm. *Optimization and Engineering* **2021**, *22*, 1539–1555, doi:10.1007/s11081-020-09534-7.
18. Ekinci, S.; Izci, D.; Abualigah, L.; Hussien, A.G.; Thanh, C.-L.; Khatir, S. Revolutionizing Vehicle Cruise Control: An Elite Opposition-Based Pattern Search Mechanism Augmented INFO Algorithm for Enhanced Controller Design. *International Journal of Computational Intelligence Systems* **2023**, *16*, 129, doi:10.1007/s44196-023-00304-8.
19. Mirjalili, S. SCA: A Sine Cosine Algorithm for Solving Optimization Problems. *Knowl Based Syst* **2016**, *96*, 120–133, doi:10.1016/j.knosys.2015.12.022.
20. Ahmadianfar, I.; Heidari, A.A.; Noshadian, S.; Chen, H.; Gandomi, A.H. INFO: An Efficient Optimization Algorithm Based on Weighted Mean of Vectors. *Expert Syst Appl* **2022**, *195*, 116516, doi:10.1016/j.eswa.2022.116516.
21. Faramarzi, A.; Heidarinejad, M.; Mirjalili, S.; Gandomi, A.H. Marine Predators Algorithm: A Nature-Inspired Metaheuristic. *Expert Syst Appl* **2020**, *152*, 113377, doi:10.1016/j.eswa.2020.113377.
22. Ekinci, S.; Izci, D.; Kayri, M. An Effective Controller Design Approach for Magnetic Levitation System Using Novel Improved Manta Ray Foraging Optimization. *Arab J Sci Eng* **2022**, *47*, 9673–9694, doi:10.1007/s13369-021-06321-z.
23. Hekimoğlu, B. Sine-Cosine Algorithm-Based Optimization for Automatic Voltage Regulator System. *Transactions of the Institute of Measurement and Control* **2019**, *41*, 1761–1771, doi:10.1177/0142331218811453.
24. Mosaad, A.M.; Attia, M.A.; Abdelaziz, A.Y. Whale Optimization Algorithm to Tune PID and PIDA Controllers on AVR System. *Ain Shams Engineering Journal* **2019**, *10*, 755–767, doi:10.1016/j.asej.2019.07.004.
25. Izci, D.; Ekinci, S.; Zeynelgil, H.L.; Hedley, J. Fractional Order PID Design Based on Novel Improved Slime Mould Algorithm. *Electric Power Components and Systems* **2021**, *49*, 901–918, doi:10.1080/15325008.2022.2049650.
26. Sahib, M.A. A Novel Optimal PID plus Second Order Derivative Controller for AVR System. *Engineering Science and Technology, an International Journal* **2015**, *18*, 194–206, doi:10.1016/j.jestch.2014.11.006.
27. Mohd Tumari, M.Z.; Ahmad, M.A.; Mohd Rashid, M.I. A Fractional Order PID Tuning Tool for Automatic Voltage Regulator Using Marine Predators Algorithm. *Energy Reports* **2023**, *9*, 416–421, doi:10.1016/j.egyr.2023.10.044.
28. Izci, D.; Ekinci, S.; Hussien, A.G. Effective PID Controller Design Using a Novel Hybrid Algorithm for High Order Systems. *PLoS One* **2023**, *18*, e0286060, doi:10.1371/journal.pone.0286060.
29. Izci, D.; Ekinci, S. An Improved RUN Optimizer Based Real PID plus Second-Order Derivative Controller Design as a Novel Method to Enhance Transient Response and Robustness of an Automatic Voltage Regulator. *e-Prime - Advances in Electrical Engineering, Electronics and Energy* **2022**, *2*, 100071, doi:10.1016/j.prime.2022.100071.

30. Ozgenc, B.; Ayas, M.S.; Altas, I.H. Performance Improvement of an AVR System by Symbiotic Organism Search Algorithm-Based PID-F Controller. *Neural Comput Appl* **2022**, *34*, 7899–7908, doi:10.1007/s00521-022-06892-4.
31. Padiachy, V.; Mehta, U.; Azid, S.; Prasad, S.; Kumar, R. Two Degree of Freedom Fractional PI Scheme for Automatic Voltage Regulation. *Engineering Science and Technology, an International Journal* **2022**, *30*, 101046, doi:10.1016/j.jestch.2021.08.003.
32. Ekinci, S.; Izci, D.; Abu Zitar, R.; Alsoud, A.R.; Abualigah, L. Development of Lévy Flight-Based Reptile Search Algorithm with Local Search Ability for Power Systems Engineering Design Problems. *Neural Comput Appl* **2022**, *34*, 20263–20283, doi:10.1007/s00521-022-07575-w.
33. Dogruer, T.; Can, M.S. Design and Robustness Analysis of Fuzzy PID Controller for Automatic Voltage Regulator System Using Genetic Algorithm. *Transactions of the Institute of Measurement and Control* **2022**, *44*, 1862–1873, doi:10.1177/01423312211066758.
34. Ayas, M.S.; Sahin, E. FOPID Controller with Fractional Filter for an Automatic Voltage Regulator. *Computers & Electrical Engineering* **2021**, *90*, 106895, doi:10.1016/j.compeleceng.2020.106895.
35. Micev, M.; Ćalasan, M.; Ali, Z.M.; Hasanien, H.M.; Abdel Aleem, S.H.E. Optimal Design of Automatic Voltage Regulation Controller Using Hybrid Simulated Annealing – Manta Ray Foraging Optimization Algorithm. *Ain Shams Engineering Journal* **2021**, *12*, 641–657, doi:10.1016/j.asej.2020.07.010.
36. Altbawi, S.M.A.; Mokhtar, A.S. Bin; Jumani, T.A.; Khan, I.; Hamadneh, N.N.; Khan, A. Optimal Design of Fractional Order PID Controller Based Automatic Voltage Regulator System Using Gradient-Based Optimization Algorithm. *Journal of King Saud University - Engineering Sciences* **2021**, doi:10.1016/j.jksues.2021.07.009.
37. Suid, M.H.; Ahmad, M.A. Optimal Tuning of Sigmoid PID Controller Using Nonlinear Sine Cosine Algorithm for the Automatic Voltage Regulator System. *ISA Trans* **2022**, *128*, 265–286, doi:10.1016/j.isatra.2021.11.037.
38. Lewis, R.M.; Torczon, V. Pattern Search Algorithms for Bound Constrained Minimization. *SIAM Journal on Optimization* **1999**, *9*, 1082–1099, doi:10.1137/S1052623496300507.
39. Tizhoosh, H.R. Opposition-Based Learning: A New Scheme for Machine Intelligence. In Proceedings of the International Conference on Computational Intelligence for Modelling, Control and Automation and International Conference on Intelligent Agents, Web Technologies and Internet Commerce (CIMCA-IAWTIC'06); IEEE, 2005; Vol. 1, pp. 695–701.
40. Ekinci, S.; Izci, D.; Eker, E.; Abualigah, L.; Thanh, C.-L.; Khatir, S. Hunger Games Pattern Search with Elite Opposite-Based Solution for Solving Complex Engineering Design Problems. *Evolving Systems* **2023**, doi:10.1007/s12530-023-09526-9.
41. Yildiz, B.S.; Pholdee, N.; Bureerat, S.; Yildiz, A.R.; Sait, S.M. Enhanced Grasshopper Optimization Algorithm Using Elite Opposition-Based Learning for Solving Real-World Engineering Problems. *Eng Comput* **2021**, doi:10.1007/s00366-021-01368-w.
42. Ekinci, S.; Izci, D.; Eker, E.; Abualigah, L. An Effective Control Design Approach Based on Novel Enhanced Aquila Optimizer for Automatic Voltage Regulator. *Artif Intell Rev* **2023**, *56*, 1731–1762, doi:10.1007/s10462-022-10216-2.
43. Izci, D.; Ekinci, S. A Novel-Enhanced Metaheuristic Algorithm for FOPID-Controlled and Bode's Ideal Transfer Function–Based Buck Converter System. *Transactions of the Institute of Measurement and Control* **2023**, *45*, 1854–1872, doi:10.1177/01423312221140671.
44. Tabak, A. Novel TIΛDND2N2 Controller Application with Equilibrium Optimizer for Automatic Voltage Regulator. *Sustainability* **2023**, *15*, 11640, doi:10.3390/su151511640.